RSC Advances

PAPER

View Article Online
View Journal | View Issue

Cite this: *RSC Adv.*, 2026, **16**, 5795

Sonochemically synthesized CuO-NPs: individual and synergistic toxicity assessment with sodium arsenite in adult zebrafish

Aqsa Huma,†[a] Ameer Hamza,†[b] Mazhar Iqbal Zafar, *[a] Muhammad Babar Taj, *[c] Zeshan Sheikh,[d] Naveed Khan,[e] Imtiaz Ahmad Khan,[f] Ahmed Atiullah[a] and Muhammad Majid[gh]

Sodium arsenite ($NaAsO_2$) and sonochemically synthesized copper oxide nanoparticles (CuO-NPs) pose escalating risks to aquatic animals due to their bio-accumulative potential, persistence, and interaction; when co-occurring, their combined effects represent a new class of emerging contaminants (ECs) with heightened ecological relevance. We synthesized CuO-NPs and characterized them using powder X-ray diffraction, scanning electron microscopy, Fourier transform infrared spectroscopy, energy dispersive X-ray spectroscopy and UV-visible spectroscopy. Zebrafish (*Danio rerio*) were exposed to $NaAsO_2$, CuO-NPs, and their combination for 28 days, and they were subjected to comprehensive histopathological analysis of muscle tissues and biochemical and genotoxic examinations on the 7th, 14th, 21st, and 28th days of exposure. The synthesized CuO-NPs exhibited an average crystallite size of 10.56 nm, with a monoclinic crystalline structure and spherical morphology. Treatment with CuO-NPs and their co-exposure with $NaAsO_2$ induced histomorphological alterations in muscle tissues, significantly elevated hepatic oxidative stress biomarkers ($P \leq 0.0001$), and suppressed total protein ($P \leq 0.05$), antioxidant ($P \leq 0.0001$), and acetylcholinesterase ($P \leq 0.0001$) enzyme activities. The imbalance of oxidants and antioxidants induced DNA damage, as revealed by the comet assay. The correlational analysis exhibited a strong, significant correlation ($P = 0.05$) among oxidative stress biomarkers, antioxidant enzyme activities, and DNA damage. These findings indicate that CuO-NPs exhibit individual and synergistic toxicity with $NaAsO_2$, highlighting their potential ecological concerns.

Received 8th December 2025
Accepted 8th January 2026

DOI: 10.1039/d5ra09469k

rsc.li/rsc-advances

1 Introduction

Emerging contaminants (ECs) in aquatic systems pose significant threats to public and environmental health and have been recognized worldwide as a major concern.[1] These contaminants include personal care products, pharmaceuticals, industrial chemicals, surfactants, plasticizers, disinfectants, detergents, alkylphenols, nanomaterials, and persistent organic pollutants.[2–11] Particularly, many of these ECs remain in environmental matrices, and they have the capacity to bioaccumulate across food webs. This contamination can impact human and animal health.[12] Endocrine disruption, interference with cellular signaling pathways, and the disruption of physiological, metabolic, and immunological processes can be induced in aquatic organisms.[13–15] The noticeable adverse effects of such processes include stunted somatic growth and disturbed neurodevelopment.[16,17] There is also potential danger from their transformation products known as secondary metabolites, which are often more toxic than the parent compounds.[18]

Rapid industrialization all over the world has greatly hastened the rate at which heavy metals and metalloids are discharged into aquatic environments, with significant consequences on human and ecological health.[19,20] Aquatic ecosystems are highly vulnerable to heavy metals since these elements are taken up by the flora and fauna in aquatic environments, manifesting toxicological consequences.[21,22] In this regard, arsenic is one of the well-documented environmental pollutants that can exhibit toxicity, induce adverse effects, and bioaccumulate.[23,24]

[a]*Department of Environmental Sciences, Faculty of Biological Sciences, Quaid-i-Azam University, Islamabad 45320, Pakistan. E-mail: mzafar@qau.edu.pk*
[b]*Department of Zoology, Quaid-i-Azam University, Islamabad 45320, Pakistan*
[c]*Institute of Chemistry, The Islamia University of Bahawalpur, Bahawalpur, Pakistan. E-mail: dr.taj@iub.edu.pk*
[d]*Institute of Environmental Sciences and Engineering (IESE), National University of Sciences and Technology (NUST), Islamabad, 44000, Pakistan*
[e]*Department of Mathematics, COMSATS University Islamabad, Park Road, Islamabad, 44000, Pakistan*
[f]*Department of Pathology, Faculty of Veterinary Sciences, PMAS-Arid Agriculture University, Rawalpindi, Pakistan*
[g]*Department of Pharmacy, Guangdong Medical University Dongguan, China*
[h]*Faculty of Pharmacy, Hamdard University, Islamabad, Pakistan*
† Equal contribution. These authors are joint first authors.

Arsenic, in its trivalent form, is of particular concern due to its geochemical cycling, anthropogenic inputs, and high toxicity. Sodium arsenite ($NaAsO_2$) is one of the most common arsenic compounds used in industrial applications and is highly bioavailable to aquatic organisms in contaminated water bodies, where it remains for longer periods and causes significant oxidative stress. Even sublethal concentrations of $NaAsO_2$ have been linked to histopathological changes, disturbances in antioxidant defenses, immunotoxicity, and genotoxic effects.[25–29] Although arsenic is present in aquatic environments, how this EC interacts with other ECs and affects aquatic organisms is poorly understood and relatively understudied.

Simultaneously, engineered nanomaterials are acting as ECs in aquatic bodies. CuO-NPs have gained significance due to their large-scale applications on industrial levels. They are chemically stable, functionally versatile, and cost-effective. CuO-NPs have excellent thermal, electronic, and dielectric characteristics, and find applications in energy storage systems, electronics, glucose sensors, photocatalysis, and antimicrobial technologies.[30,31]

Despite their industrial appeal, a critical gap remains in the toxicological evaluation of sonochemically synthesized CuO-NPs on aquatic fauna. Additionally, how these nanoparticles interact with other environmental pollutants, such as $NaAsO_2$, is not well understood. To the best of our knowledge, to date, all the existing studies have addressed the physicochemical characteristics and material efficiency of CuO-NPs while overlooking their interactions with biological systems, particularly in freshwater fauna. Moreover, no study has evaluated their combined effects with already persisting chemicals, *e.g.*, $NaAsO_2$, in freshwater bodies. We used zebrafish as a model organism due to their presence in freshwater ecosystems and their physiological similarity to human beings.

It is well understood that CuO-NPs have the potential to induce toxicological effects in zebrafish, positioning them as an emerging aquatic contaminant when they interact with $NaAsO_2$. Co-exposure to these contaminants amplifies histopathological anomalies, oxidative stress, and genotoxicity, while simultaneously depressing the antioxidant defense system. The CuO-NPs differ significantly in their physicochemical properties from $NaAsO_2$; their comparison presents systematic insights into the relative and combined toxicological effects of nanomaterial particulates and dissolved metal ions commonly found in the aquatic environment. Toxicity from such co-exposure is expected to be manifested as synergistic toxicological interactions, reflecting real-world contaminant mixtures. This investigation aims to study and compare the toxicological effects of $NaAsO_2$ and CuO-NPs in adult zebrafish. Key objectives include synthesizing CuO-NPs using sonochemical methods, characterizing them with UV-Vis spectroscopy, PXRD, SEM-EDX, and FTIR, assessing histopathological changes in skeletal muscle tissues at different exposure levels, and examining oxidative stress markers, antioxidant responses, and genotoxic effects using the comet assay. This study will help to understand the damage caused by CuO-NPs in freshwater aquatic systems, develop regulatory frameworks, and contribute to attaining Sustainable Development Goals 6 and 15.

"We would like to clarify that the sonochemical synthesis of CuO-NPs is indeed a well-established technique, and we do not claim intrinsic novelty in the synthesis procedure itself. The chemical novelty of the present work lies in employing sonochemically synthesized CuO-NPs with distinct surface and structural features to investigate their comparative and synergistic toxicological interactions with $NaAsO_2$. To the best of our knowledge, such a combined toxicity assessment, linking synthesis-dependent physicochemical characteristics of CuO-NPs to arsenic-mediated toxicity enhancement, has not been previously reported."

2 Materials and methods

2.1 Chemicals

$NaAsO_2$ (CAS: 7784-46-5; purity 99%) was obtained from Fluka Chemika; dimethyl sulfoxide (DMSO) from Honeywell Company (Morristown, NJ, USA); acetylthiocholine iodide (CAS: 2260-50-6; purity 99.0%) and nitrotetrazolium blue chloride (NBT) (CAS: 298-83-9; purity 98%) from Sigma Aldrich® (Germany); ethylenediamine tetra acetic acid (EDTA) (CAS: 60-00-4; purity 99%) from Sigma Aldrich, Germany, H_2O_2 (CAS: 7722-84-1); riboflavin (CAS: 83-88-5; purity 98%), copper nitrate, and copper chloride from Merck (Darmstadt, Germany). All other chemicals used in the experimental work were of analytical grade.

2.2 Sonochemical synthesis of CuO-NPs

The CuO-NPs were synthesized by the well-known sonochemical method, with slight modification.[32] The CuO-NPs were prepared by dissolving 1 g of copper chloride in 200 mL of aqueous solution. The solutions were sonicated by a probe sonicator (20 kHz, 750 W, 35% amplitude). When the temperature reached 60 °C, an aqueous solution of sodium hydroxide was added to adjust the pH to 8. The sonication was conducted for 30 min. The resultant solution was centrifuged, washed with water, and dried at 60 °C overnight.

2.3 Characterization of CuO-NPs

2.3.1 Powder X-ray diffraction. The crystalline structure of the NPs was characterized by PXRD using a 2.2 kW Cu anode ceramic X-ray tube at a wavelength of 1.54 Å. The scans were performed over a 5–70° range, and the results were compared with the Joint Committee on Powder Diffraction Standards (JCPDS) database to confirm the crystalline structure. The crystallite size was determined using the Debye–Scherrer equation:[33]

$$D = \frac{k\lambda}{\beta \cos \theta} \quad (1)$$

In eqn (1), "D" denotes the crystallite size of CuO-NPs, "k" is the Scherrer constant, "λ" is the wavelength of the X-ray source, "β" represents the full width at half maximum (FWHM) of the diffraction peak, and "θ" is the Bragg angle.

2.3.2 Fourier transform infrared spectroscopy. The functional groups of CuO-NPs were analyzed using FTIR spectroscopy (FTIR-6600 type A, Jasco). The NPs pellet was prepared

using KBr (7000PSI), and the FTIR spectrum (4000–400 cm^{-1}) was analyzed using Origin Pro 8.5.

2.3.3 Morphological analysis. The particle size and morphology of CuO-NPs were determined using SEM (EV018 Carl Zeiss, Germany). A 10 mg L^{-1} suspension of NPs was coated on a glass slide, sputtered with gold after drying, and subsequently examined under a high-magnification SEM prior to energy dispersive X-ray spectroscopy (EDX) analysis. The EDX analysis was used to determine the elemental composition of NPs.

2.3.4 Ultraviolet visible spectroscopy. UV-visible spectroscopy was performed to confirm the formation of CuO-NPs using a Thermo Fisher Scientific UV-Vis Spectrophotometer (Type 1510).

2.3.5 Zeta potential and zeta sizer. The zeta potential (ZP) and hydrodynamic diameter of CuO-NPs in their original dissolution medium (DMSO) and in combination with $NaAsO_2$ were assessed using a Malvern Zetasizer Nano ZS.

2.4 Experimental design

The current experiment was performed in the Environmental Toxicology and Chemical Risk Assessment Laboratory, Quaid-i-Azam University, Islamabad, Pakistan. Wild-type AB strain adult zebrafish were cultured and maintained in the laboratory. The fish were acclimatized for 14 days in dechlorinated water prior to the experiment. The dissolved oxygen levels (7.0 ± 1.0 mg L^{-1}), a light–dark cycle (14:10 h), temperature (27.0 ± 1.0 °C), and pH (7.4–8.1) were maintained. The fish were fed daily at 5% body weight with Optimum Betta (commercial fish food). The water in the treatment tanks was changed on alternate days to ensure quality and contaminant concentrations.

The experiment assessed the effects of sub-lethal toxicity from individual exposures and co-exposures of $NaAsO_2$ and CuO-NPs on the zebrafish. A total of 480 fish were randomly assigned to one control and three treatment groups. The control group did not receive any treatment. Treatment group 1 (T1) was exposed to $NaAsO_2$ (300 μg L^{-1}), treatment group 2 (T2) was administered with 1 mg L^{-1} of CuO-NPs, and treatment group 3 (T3) was simultaneously exposed to $NaAsO_2$ and CuO-NPs (300 μg L^{-1} and 1 mg L^{-1}, respectively). DMSO (0.001%) served as the dissolution medium for NPs, as this concentration has been recommended as safe for chronic exposure,[34] and this is far below the reported safe threshold in acute (1%) and sub-chronic (0.1%) toxicity for 14 days.[35,36] On days 7, 14, 21, and 28 of exposure, 30 fish from each group were sacrificed *via* the ice-induced shock killing method, dissected, and the organs were collected. Samples were stored in PBS (pH 7.4) at −80 °C, while muscle tissues were preserved in neutral buffered formalin at 4 °C. The key experimental protocols are shown in Fig. 1.

2.5 Selection criteria and concentration of dosage solutions

The test concentrations of $NaAsO_2$ and CuO-NPs were chosen to reflect both environmentally relevant levels and previously reported sublethal exposure ranges in zebrafish. The World Health Organization (WHO) guideline for arsenic in drinking water is 10 μg L^{-1}; aquatic organisms such as zebrafish are often exposed to substantially higher concentrations in contaminated surface waters. In Pakistan, elevated As levels have been reported, ranging from 360–683 μg L^{-1} in surface water and 1–525 μg L^{-1} in groundwater.[37,38] Therefore, to evaluate the sublethal effects under environmentally relevant conditions, the test concentration of As (300 μg L^{-1}) was selected based on a report by Hallauer *et al.*,[39] who demonstrated chronic toxicity in zebrafish across 50–300 μg L^{-1}. The CuO-NPs (1 mg L^{-1}) were adopted in accordance with Mani *et al.*,[40] who reported sublethal toxic effects with commercially synthesized NPs. These selected concentrations were further supported by environmental levels and toxicity thresholds.[41,42]

2.6 Skeletal muscle histopathology

Histopathological alterations in ZF skeletal muscle tissues were examined using the hematoxylin and eosin (H&E) staining procedure. The histopathological slide was prepared, involving various steps: fixation, dehydration, embedding, slide preparation, staining, and microscopy, according to the previously established standardized protocols of our laboratory.[33] An Olympus-CX41 microscope attached to a Tucson camera was used to observe and capture histopathological changes on slides at ×100 magnification.

2.7 Biochemical analysis

2.7.1 Homogenate preparation. Hepatic tissues were homogenized in 50 mM potassium PB (pH 7.0) using a Precellys homogenizer (Bertin Technologies). The homogenates were centrifuged at 10 000 rpm for 10 min and the supernatant was collected. All biochemical assays were performed in triplicate, and the average of replicates was computed and subsequently used for all statistical analyses.

2.7.2 Quantification of total protein content. The total protein content in zebrafish liver was quantified using the Sigma Bradford method with bovine serum albumin (BSA) as the standard, and a few modifications to the existing protocol.[43] Five BSA dilutions (10, 20, 40, 60, 80, and 100 μg mL^{-1}) were prepared to draw a standard curve, and the absorbance was measured at 595 nm on a UV-visible spectrophotometer (Cecil 7500). The concentration of protein was calculated using the standard curve $Y = 0.0053X + 0.0306$. The estimation of total protein was expressed in μg mL^{-1}.

2.7.3 Quantification of total reactive oxygen species (ROS). The methodology employed for evaluating ROS in the liver tissue of zebrafish was based on the protocol described by Hayashi *et al.*[44] Briefly, the ROS concentration was quantified using 0.1 M sodium acetate, *N*,*N*-diethyl-*p*-phenylenediamine (DEPPD), and $FeSO_4$ in a 96-well plate. The standard curve was generated using H_2O_2 and the final concentration was expressed in nM per mg protein.

2.7.4 Quantification of malondialdehyde (MDA). The MDA concentration was assessed following the protocols of Iqbal and Wright, with a few modifications.[45,46] The reaction mixture was comprised of 0.58 mL of PB (0.1 M, pH 7.4), ascorbic acid (0.1 M), 0.02 mL of $FeCl_3$ (0.1 M), and 200 μL of tissue homogenate, and was incubated for 1 h at 37 °C. The reaction was stopped

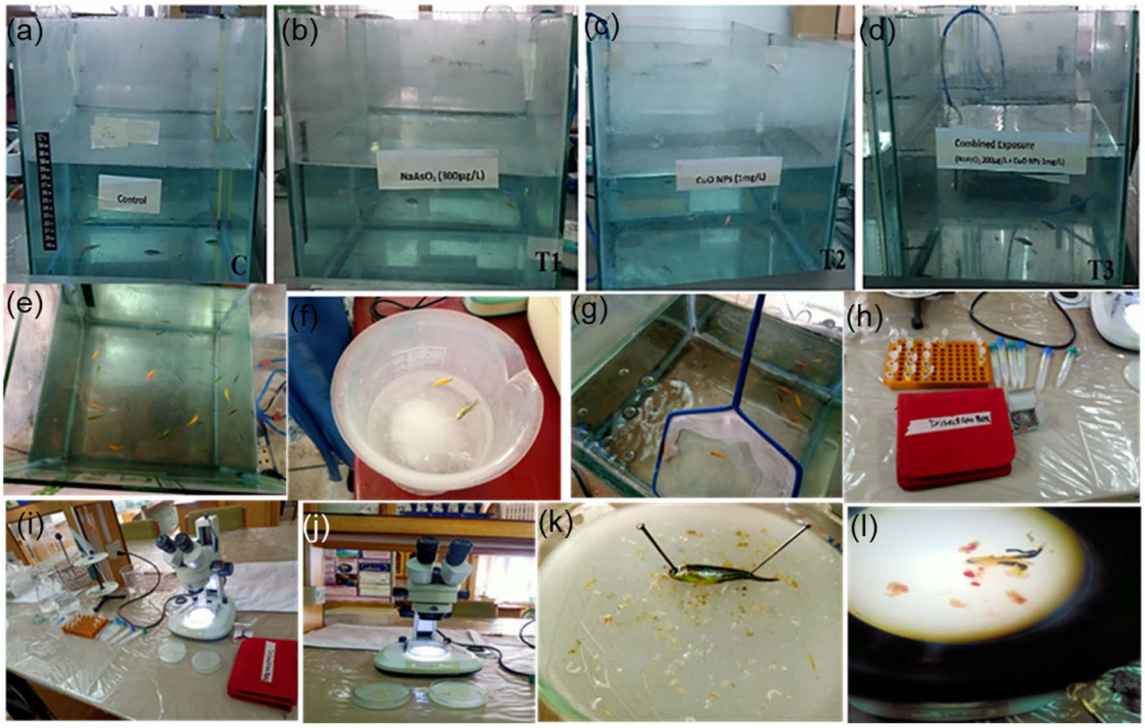

Fig. 1 Macroscopic representations of key experimental protocols and setups. Aquariums of the (a) control group, (b) $NaAsO_2$-treated group, (c) CuO-NP-treated group, and (d) $NaAsO_2$ + CuO-NP-treated group. (e) Zebrafish moving in the aquarium. (f) Ice-shock killing method. (g) Collection of zebrafish from the aquarium using a fish net. (h) Preparations for dissection, including a dissection box, Eppendorf tubes for collecting organs, and Falcon tubes for collecting fish. (i & j) Stereomicroscope in working state. (k) Zebrafish in a dissecting Petri dish. (l) Organ view from the eyepiece of the microscope.

with 10% W/V trichloroacetic acid, followed by the addition of a 0.67% W/V solution of thiobarbituric acid, and heated in boiling water for 30 min. After cooling and centrifugation, the optical density at 532 nm was recorded, and the concentration of malondialdehyde (MDA) was expressed as nM per mg of proteins.

2.7.5 Estimation of superoxide dismutase (SOD) activity. The SOD activity was measured, following previously established protocols with minor modifications.[47] Briefly, 50 µL of tissue homogenate was mixed with 50 mM PB (pH 7.8), 100 µL of EDTA, 130 µL of methionine, 750 µL of NBT, and 20 µL of riboflavin and incubated. The enzyme activity was determined by monitoring the change in absorbance at 560 nm, and is expressed as U per mg of protein.

2.7.6 Estimation of catalase (CAT) activity. The CAT activity was quantified according to the previously reported protocols.[48] Briefly, the reaction mixture, comprising 200 µL PB (50 mM, pH 7.6) and 20 µL H_2O_2 (30 mM), was placed in a test tube. Next, 100 µL of homogenate solution was dispensed into the reaction mixture, and the CAT activity was assessed by measuring the absorbance at 240 nm using a spectrophotometer (Thermo Scientific Spectrophotometer UV-3100PC), expressed as U per mg of protein.

2.7.7 Quantification of acetylcholinesterase (AChE). The AChE activity in brain homogenate was measured spectrophotometrically using a UV spectrophotometer (Model: T80+) at 412 nm. Briefly, 50 µL of tissue homogenate was mixed with 0.5 M PB (pH 7.8), 1% sodium citrate, 50 µL of 0.5 mM DTNB, 50 µL of 10 mM acetylthiocholine iodide, and distilled water (650 µL) and incubated. The AChE activity was denoted in U min^{-1}.

2.8 Comet assay

The evaluation of DNA damage in zebrafish liver tissues was conducted through single-cell gel electrophoresis by employing the comet assay method. The reagents for the assay, including low-melting agarose (LMA), standard melting agarose (SMA), lysing solution, electrophoresis buffer, neutralization buffer, staining solution, and PBS buffer, were prepared carefully. The slides were cleaned, disinfected, and coated with SMA and LMA layers, followed by immersing in the lysing solution and chilling. Electrophoresis was carried out, involving the application of power, neutralization, staining with ethidium bromide, and covering with slips. The positive control for this assay was ethyl methane sulfonate. The slides were visualized using a fluorescence microscope (Nikon) at ×400, and CASP 1.2.3.b software facilitated the assessment of DNA damage levels. The analysis involved examining DNA migration in each cell, and results were recorded by comparing DNA transfer and the proportion of cells exhibiting high DNA fragment migration ratios.

2.9 Statistical and mathematical analysis

All the experimental procedures were performed in triplicate for each treatment group, and the results are presented as means ±

SD. The statistical analysis was performed using GraphPad Prism version 9.5.1 and Anaconda Python. One-way analysis of variance (ANOVA) determined the statistical significance between the treatments and control groups. The normal distribution and homogeneity of variances were checked. Tukey's *post hoc* test was employed to compare the means within groups. One-way ANOVA was applied as each fish was sacrificed at a distinct time, no individual was followed longitudinally, and each time point denoted an independent biological endpoint. The level of significance was adjusted to $p < 0.05$. Matplotlib was used for data visualization. The Bliss independence model was employed to prove the synergy in biochemical parameters. The exact mathematical equations of the Bliss independence model to infer synergistic and antagonistic interactions using a single concentration and combination of $NaAsO_2$ and CuO-NPs are given in SI (Section 1). The statistical significance of the predictors was also assessed based on the *p*-values in each model.

3 Results

3.1 Characterization of CuO-NPs

3.1.1 Powder X-ray diffraction. The PXRD pattern had intense peaks at 2θ positions of 32.5°, 35.4°, 35.5°, 38.7°, 38.9°, 46.3°, 48.8°, 51.3°, 53.5°, 58.3°, 61.5°, 65.2°, 66.3°, and 68.1°, corresponding to (110), (002), (−111), (111), (200), (−112), (−202), (112), (020), (202), (−113), (022), (−311), and (220) planes, respectively, representing the monoclinic crystal system of CuO-NPs (JCPDS card no. 00-005-0661). The absence of impurity peaks indicated the high quality of the CuO-NPs, as shown in Fig. 2a. The average crystallite size of the NPs was 10.56 nm, which was calculated and presented in Table S1.

3.1.2 Morphological analysis. The surface morphology of the synthesized CuO-NPs was examined using SEM. The SEM micrographs showed that the NPs were spherical with uniform distribution. The average particle size was 41.66 nm. The CuO-NPs were well dispersed, with no agglomeration, indicating their high stability. The NPs demonstrated clear boundaries and well-defined morphology as shown in Fig. 2b.

3.1.3 Fourier transform infrared spectroscopy. The broad spectral band at 3401 cm^{-1} corresponds to –OH stretching vibrations attributed to the adsorbed water molecules on the surface of nanocrystalline CuO, probably due to their high surface area. The peak observed around 1620 cm^{-1} was assigned to the bending vibrations of H–O–H from surface-adsorbed moisture. The sharp peak at 1112 cm^{-1} corresponds to carbonate or bicarbonate stretching, suggesting the possible CO_2 encapsulation on the surface of NPs. The intense peaks at 597 and 512 cm^{-1} are characteristic of Cu(II)–O stretching vibrations, confirming the formation of CuO-NPs as shown in Fig. 2c.

3.1.4 Energy dispersive X-ray spectroscopy. The EDX spectrum confirmed the elemental composition of CuO-NPs. The EDX spectrum depicted strong signals of Cu (73%), O (21%), and C (5.7%). The minor carbon peak might be due to the carbon coating used during sample preparation for SEM analysis. There were no other elemental peaks present in the spectrum, suggesting the high purity of the newly synthesized NPs, as shown in Fig. 2d.

3.1.5 Ultraviolet visible spectroscopy. The UV-visible spectroscopy results indicated that CuO-NPs demonstrated a sharp and intense absorption peak at 250 nm (Fig. 2f). The observed surface plasmon resonance band (SPR) corresponds to the charge transfer transition between O^{2-} and Cu^{2+} ions, confirming the successful synthesis of CuO-NPs. The CuO-NPs typically show absorbance peaks in the 280 nm to 300 nm range. The pronounced blue shift towards the shorter wavelength may be due to quantum confinement effects. The absence of additional absorbance peaks highlights the high purity of CuO-NPs and the absence of secondary Cu phases such as Cu_2O.

3.1.6 Zeta potential and zeta sizer. ZP provides information about the electrical state of charged interfaces. A higher negative or positive ZP value is an indicator of strong electrostatic repulsion between the particles. The CuO-NPs in their dissolution medium (DMSO) exhibited a ZP of −17.9 mV. The CuO-NPs, following treatment with $NaAsO_2$, exhibited a slight reduction in the ZP value, *i.e.*, −16.0 mV. The magnitude of this reduction is small; however, it indicates partial neutralization of the surface and a decrease in the electrostatic repulsion between the NPs. The observed reduction may be due to the electrostatic screening effect triggered by possible surface interactions of $NaAsO_2$ with the functional groups on the CuO-NPs surface.

The zeta sizer results also demonstrated that the CuO-NPs in DMSO had an average hydrodynamic diameter of 183.5 nm and polydispersity index (PDI) of 0.12, indicating the monodisperse nature of CuO-NPs. The average size and PDI of NPs increased from 183.5 d.nm to 301.5 d.nm and 0.12 to 0.374, respectively, after the addition of $NaAsO_2$. This change might be associated with an increase in the ionic strength of the solution, which compressed the electrical double layer surrounding the NP surface, thereby weakening the electrostatic repulsion force and favoring interparticle attraction. Consequently, enhanced agglomeration and hetero-association of CuO-NPs occurred, leading to a large hydrodynamic diameter as detected by the zeta sizer. The results are shown in Fig. 3a–d.

3.2 Water quality parameters

In the present study, water quality parameters including temperature, electrical conductivity (EC), total dissolved solids (TDS), dissolved oxygen (DO), and pH were systematically monitored at 12 h intervals over the 28-day exposure period. The consolidated data are summarized in Table 1. All measured values consistently remained within the optimal range for zebrafish husbandry under controlled laboratory conditions, thereby ensuring that the water quality did not disturb experimental outcomes.

3.3 Mortality observation

No mortality was recorded in either the control or treatment groups during the 28-day exposure period. Additionally, there were no physiological, morphological, or feeding behavior anomalies detected in any group.

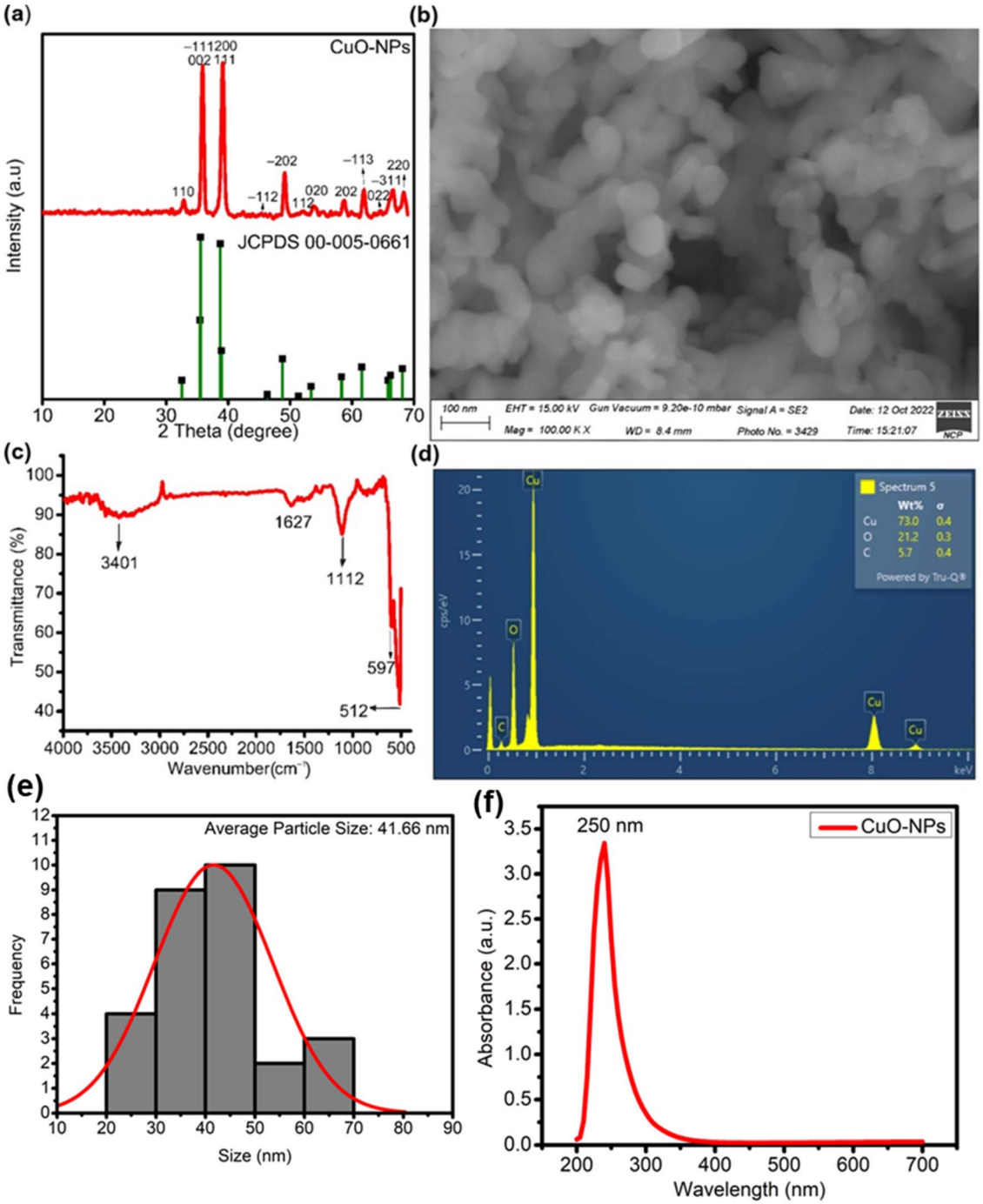

Fig. 2 Characterization of CuO-NPs: (a) PXRD pattern of CuO-NPs, (b) SEM micrographs, (c) FTIR spectrum, (d) EDX spectrum highlighting the highest content of Cu metal in CuO-NPs, (e) histogram showing particle size distribution, and (f) UV-Vis spectrum of CuO-NPs.

3.4 Histopathological analysis

A distinct pattern of muscular anomalies was observed across all the treatment groups when compared with the control. Typical well-organized cross-sections having intact myofibers, minimum interstitial space, and peripherally located nuclei were observed in the control group. $NaAsO_2$ induced necrosis, interstitial edema, myofiber swelling, and muscular atrophy. Structural deformities, particularly widespread myolysis, necrosis, and fragmentation of muscle fibers, were evident in the CuO-NP-treated group. However, co-exposure exacerbated the intensity of the damage, featuring necrosis, bioaccumulation, and fibrotic breakage. These anomalies intensified in a time-dependent manner, signifying synergistic toxicity in co-exposure groups. The extent of muscular damage is shown in Table 2 and Fig. 4.

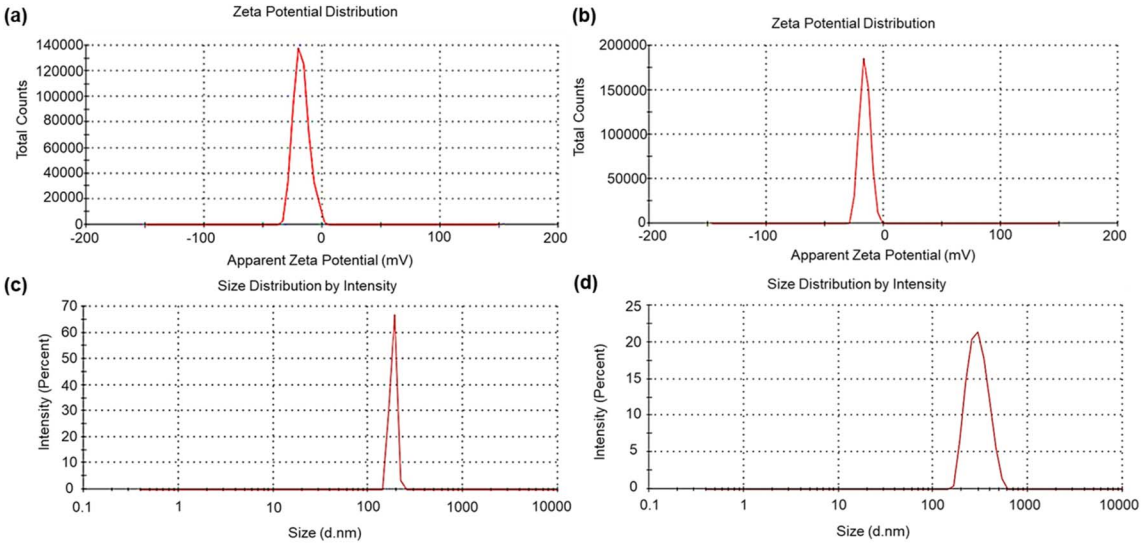

Fig. 3 . Zeta potential and hydrodynamic diameter distribution of CuO-NPs in DMSO and $NaAsO_2$-exposed conditions, respectively. (a) Zeta potential of CuO-NPs in DMSO, (b) zeta potential of CuO-NPs in $NaAsO_2$, (c) hydrodynamic diameter of CuO-NPs in DMSO, and (d) hydrodynamic diameter of CuO-NPs in $NaAsO_2$.

Table 1 Physicochemical parameters of water for the four treatments during the whole experimental period[a]

Treatments	Temperature (°C)	EC (μs cm^{-1})	TDS (mg L^{-1})	DO (mg L^{-1})	pH
Control	25.10 ± 2.54	377.50 ± 14.84	266.50 ± 13.43	6.60 ± 0.56	7.38 ± 0.16
T1	25.05 ± 2.47	373.50 ± 21.92	263.00 ± 14.14	6.75 ± 0.77	7.37 ± 0.32
T2	25.45 ± 2.89	373.50 ± 12.02	264.50 ± 10.60	6.65 ± 0.77	7.45 ± 0.35
T3	25.00 ± 2.54	370.00 ± 16.97	263.50 ± 12.02	6.55 ± 0.77	7.45 ± 0.35

[a] All values of parameters are expressed as mean ± SD.

3.5 Biochemical studies

3.5.1 Total protein estimation. The total proteins were assessed over 28 days following different treatments compared to the control group. The control group consistently exhibited higher protein concentrations relative to all treated groups, with T3 showing the more pronounced reduction over the 28-day period. Although T3 consistently exhibited the lowest protein levels, no statistically significant difference was detected among the T1, T2, and T3 groups. By days 21–28, total protein levels remained suppressed in all treated groups compared to the control. These results indicated a time-dependent decline in total protein levels, particularly in the T3 group, suggesting a strong inhibitory effect on hepatic protein synthesis. The changes in the protein levels are shown in Fig. 5a.

3.5.2 Reactive oxygen species. ROS levels significantly and time-dependently increased from day 7 to day 28 for all treatment groups ($P \leq 0.05$ to $P \leq 0.0001$). On day 7, ROS production was significantly higher in groups T1, T2, and T3 compared to the control, a pattern which continued through days 14 and 21. Notably, group T3 consistently produced the highest ROS levels at all time points measured. These findings indicated a treatment-dependent induction of oxidative stress, characterized by a progressive and sustained increase in ROS generation, with co-exposure (T3) eliciting the most pronounced response, as shown in Fig. 5b.

3.5.3 Malondialdehyde content. MDA is a biomarker of lipid peroxidation and it exhibited a similar pattern to that of ROS dynamics in response to treatments, confirming elevated MDA levels in tissue homogenates. The MDA levels significantly increased in all treatment groups in comparison to the control group ($P \leq 0.001$ for T1 and T2, $P \leq 0.0001$ for T3). The highest lipid peroxidation was observed in the T3 group from day 7 to day 28. In all treatment groups, there was also an increase in the MDA content with the duration of exposure, as shown in Fig. 5c.

3.5.4 Superoxide dismutase activity. The SOD activity demonstrated treatment and time-dependent modulations as shown in Fig. 5d. On the 7th day, T1 exhibited significantly modulated SOD activity ($P \leq 0.05$), inducing a compensatory effect. As T2 and T3 groups faced the highest oxidative stress, the SOD levels remained significantly reduced, indicating a compromised antioxidant defense mechanism. There was downregulation in SOD activity across all treatment groups on days 14, 21 and 28. Among all treatment groups, the lowest enzymatic activity was observed in the T3 group, reaching its minimal levels on the 28th day of exposure.

3.5.5 Catalase activity. The CAT activity followed a similar pattern to that of SOD, exhibiting progressive suppression

Table 2 Time-dependent progression of histopathological alterations in skeletal muscles in zebrafish following exposure to $NaAsO_2$ and CuO-NPs and their co-exposure[a]

Treatment	Necrosis (N)	Myolysis (M)	Edema (E)	Swelling (Sw)	Delocalized nuclei (DLN)	Satellite cells (S)	Bio-accumulation (A)
Day 7							
Control	–	–	–	–	–	+	–
T1	+	–	+	–	–	+	–
T2	+	+	–	+	–	+	–
T3	++	–	+	++	++	+	+
Day 14							
Control	–	–	–	–	–	+	–
T1	++	++	+	++	+	+	–
T2	++	++	+	+++	+	+	–
T3	+++	++	+	++	+++	+	–
Day 21							
Control	–	–	–	–	–	+	–
T1	+++	++	+	+++	+	+	–
T2	+++	++	+	++	++	+	–
T3	++++	++	+	++	+++	+	–
Day 28							
Control	–	–	–	–	–	+	–
T1	++++	+++	+	++++	++++	+	–
T2	+++	++	+	++	++	+	–
T3	+++++	++++	++	+++++	+++++	++	+

[a] Absence of any histopathological change is denoted as "–", "+" indicates mild changes, "++" moderate alteration, "+++" severe damage, "++++" and "+++++" represent very severe and extensive damage, respectively. For each treatment group, twenty random sections were examined. The scoring was marked in a double-blinded manner without knowledge of the treatment group or slide number. Five fish per group were examined (10 different randomly selected sections per fish) at each sampling time point. Each section was scored independently by two observers, and the values presented in this table represent the average of their scores.

across all treatment groups. There was an overall decrease in CAT activity observed over the 28 days of exposure. On the 7th day, a significant reduction in CAT activity was observed in the T3 group ($P \leq 0.0001$), as shown in Fig. 5e. A significant decrease in T1 ($P \leq 0.01$), T2 ($P \leq 0.0001$), and T3 ($P \leq 0.0001$) was also evident on day 14 and this declining trend persisted through days 21 and 28, with T3 demonstrating the highest inhibition. These results indicated that prolonged exposure suppressed CAT activity and weakened the cell's capacity to detoxify H_2O_2.

3.5.6 Acetylcholinesterase activity. Temporal changes in acetylcholinesterase activity with treatments demonstrated potential neurotoxicity. The enzyme activity was significantly decreased in all treated groups compared with the controls by day 7; T3 showed the highest inhibition, at $P \leq 0.0001$. There were similar significant reductions in T1 and T2, showing early signs of disruption of cholinergic function. These developed further and persisted on days 14, 21, and 28. The T3 group consistently had the lowest AChE activities on all days of sampling. This progressive decline in AChE activity indicated time-dependent and treatment-dependent neurotoxicity induction, likely mediated by accumulating oxidative stress. In conclusion, these results suggest that $NaAsO_2$ and CuO-NPs synergistically inhibited AChE activity and impaired cholinergic neurotransmission. The changes in AChE activity are shown in Fig. 5f.

3.6 DNA damage

DNA damage was assessed in zebrafish liver tissues using the comet assay across four time periods (days 7, 14, 21, and 28). In the control group, the comet parameters remained relatively stable, having minimum tail lengths and tail moments. Contrarily, all treatment groups presented progressive and treatment-dependent increases in DNA damage. By day 28, the T3 group exhibited the most pronounced effects, with significantly extended tail lengths (17.50 ± 2.03 μm), reduction in head lengths (23.20 ± 2.81 μm), elevated DNA percentage in the tail ($42.10 \pm 3.17\%$), and the highest tail moment (0.98 ± 0.12 μm), which are indicators of severe DNA strand breakage. The T1 and T2 groups presented less severe DNA damage in comparison to the T3 group. All the genotoxic changes in different groups at different periods are presented in Table 3 and Fig. 6.

3.7 Time and treatment-dependent effects of oxidative stress and antioxidant enzyme response

The severity of damage was assessed in the context of time; the impacts of treatment with $NaAsO_2$, CuO-NPs, and their co-exposure on oxidative stress biomarkers and the antioxidant defense mechanism in the zebrafish hepatic system were evaluated using linear regression over 28 days. A marked increase in ROS levels was observed, with effect size ranging from 12.5 to 18

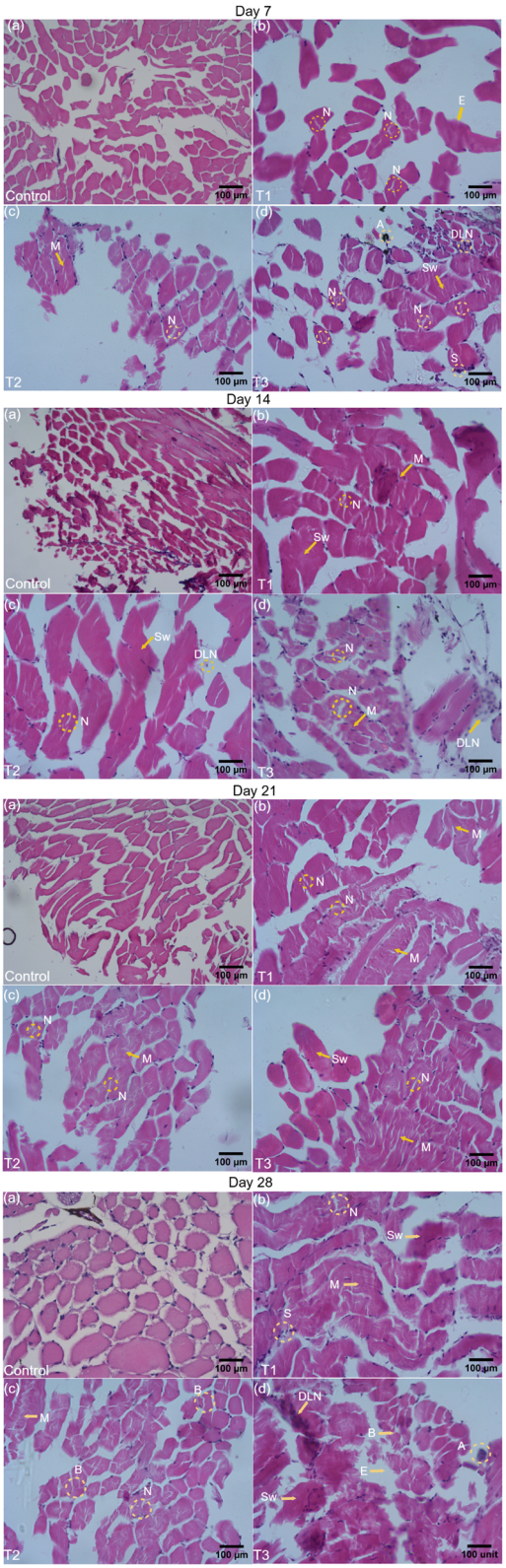

Fig. 4 Representative photomicrographs depicting time-dependent histopathological changes in skeletal muscle of adult zebrafish induced by $NaAsO_2$, CuO-NPs and their co-administration. At each time point (7, 14, 21, and 28 days), panels (a–d) correspond to the following treatments (a) control, (b) $NaAsO_2$, (c) CuO-NPs, and (d) combined $NaAsO_2$ + CuO-NPs treated groups. Scale bar = 100 µm. Abbreviations: A = accumulation of CuO-NPs, B = breakage of muscular fiber, E = edema, M = myolysis, N = necrosis, S = satellite cells, Sw = swelling, and DLN = delocalized nuclei.

by day 28 (R^2 = 0.72), indicating a strong time-dependent oxidative response (Fig. 7a). Similarly, MDA levels exhibited a progressive rise, with effect size peaking on day 28 (R^2 = 0.65), suggesting sustained membrane oxidative damage (Fig. 7b).

In contrast, antioxidant enzyme activities exhibited significant suppression across all treatment groups. Superoxide dismutase (SOD) manifested an initial compensatory response to oxidative stress in the $NaAsO_2$- and CuO-NP-treated cohorts, which was followed by a marked decline over time. The level of inhibition increased notably by day 21 (effect size < −12, R^2 = 0.64) and by day 28 (effect size < −15, R^2 = 0.54), indicating a lowered ability to neutralize superoxide radicals (Fig. 7c). Catalase (CAT) also showed progressive decline, and effect sizes had reached −15 and R^2 = 0.66 by day 28, which underscores mitochondrial susceptibility to continued oxidative stress (Fig. 7d). Altogether, the results indicated that oxidative stress mounted over time, while the antioxidant defense system progressively collapsed under the respective and combined toxicant exposures.

The oxidative damage was further quantified according to the treatment modality, suggesting that the T3 group elicited the most intensive biochemical responses. As shown in the percent change graphs in Fig. 7e–h, T3 exposure caused an 85–110% increase in ROS and MDA levels by day 28. Meanwhile, the activities of SOD and CAT were reduced by 55% and 48%, respectively. These results collectively imply that oxidative stress in the zebrafish liver increased with prolonged duration and was significantly enhanced under co-exposure conditions, emphasizing possible synergistic toxicity between $NaAsO_2$ and CuO-NP.

3.8 Pearson correlation analysis between the oxidative stress biomarkers, antioxidant enzymes and DNA damage

The correlation analysis exhibited significant associations among oxidative stress biomarkers (ROS and MDA), antioxidant enzymes (SOD and CAT) and DNA damage (TM) across different treatment groups Fig. 8. There was a strong positive correlation between ROS and MDA in all treatments: T1 (r = 0.72), T2 (r = 0.74), and T3 (r = 0.71), indicating that lipid peroxidation increased in tandem with elevated ROS. Similarly, ROS levels were positively correlated with TM in T1 (r = 0.61), T2 (r = 0.62) and T3 (r = 0.80), suggesting that increased oxidative stress was closely linked to DNA fragmentation. A comparable trend was seen between MDA and TM with r = 0.59, 0.75, and 0.92 in T1, T2, and T3, respectively, highlighting the genotoxic consequences of lipid peroxidation. In contrast, significant negative correlations were observed between ROS and antioxidants. The ROS was negatively correlated with SOD in T1 (r = −0.86); T2 (r = −0.71); and T3 (r = −0.87), with CAT in T1 (r = −0.65); T2 (r = −0.81); and T3 (r = −0.80), indicating the suppression of enzymatic defenses in response to oxidative burden. MDA also exhibited strong negative correlations with SOD in T1 (r = −0.66); T2 (r = −0.71); T3 (r = −0.64), with CAT in T1 (r = −0.73); T2 (r = −0.84); and T3 (r = −0.72).

Collectively, these results have shown a highly interrelated oxidative stress response to the experimental treatments;

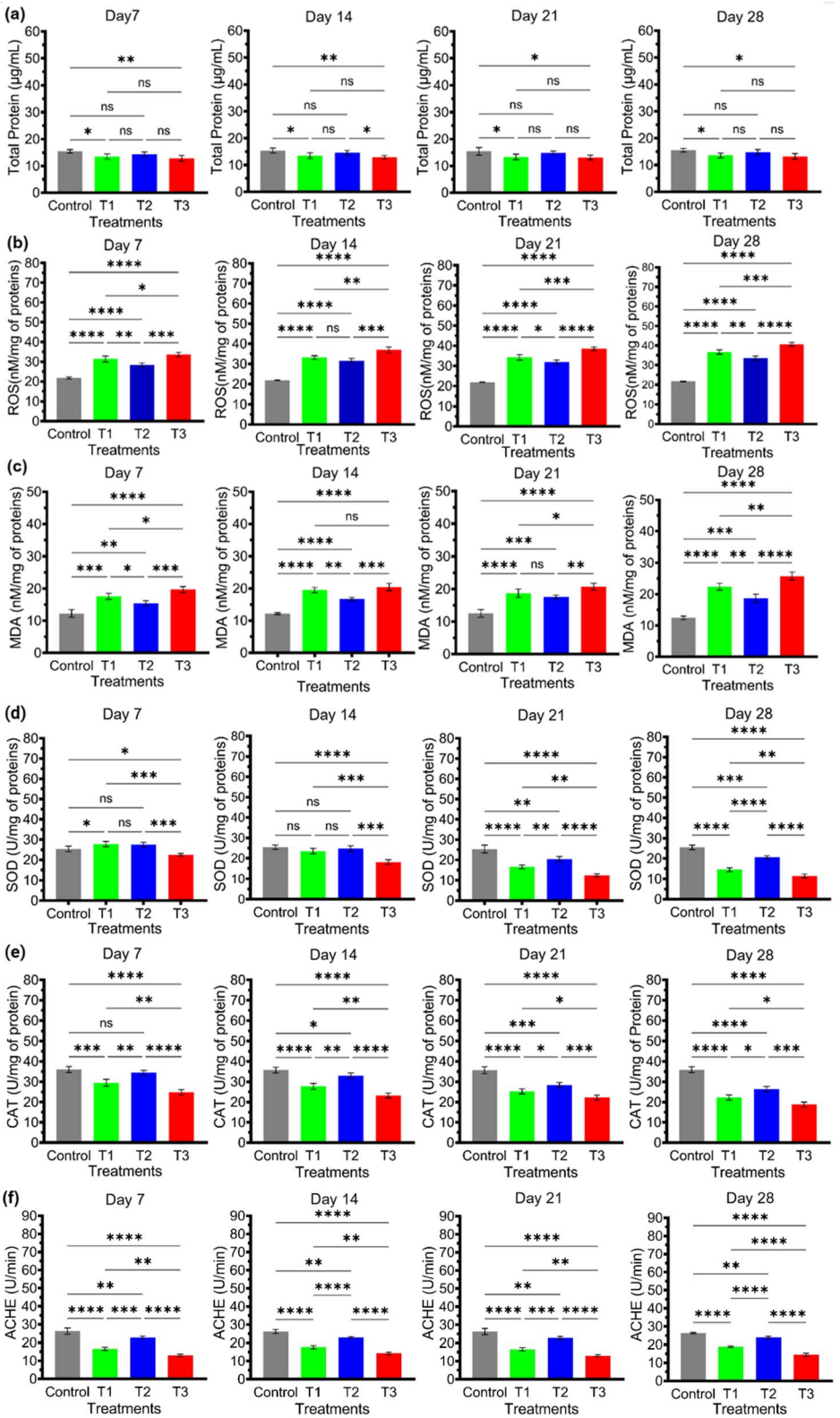

Fig. 5 Temporal modulation of hepatic and neural biochemical indices following exposure to $NaAsO_2$ and CuO-NPs and their co-exposure in adult zebrafish. (a) Alterations in hepatic total protein levels. (b) and (c) Oxidative stress biomarker concentrations. (d) and (e) Antioxidant activity. (f) Acetylcholinesterase activity. The values are expressed as mean ± SD. Significance levels are shown using "*" and they are indicated as $*P \leq 0.05$, $**P \leq 0.01$, $***P \leq 0.001$, $****P \leq 0.0001$.

Table 3 DNA damage assessment *via* comet assay in different treatment groups over the experimental period of 28 days

Treatment groups	Comet length (μm)	Head length (μm)	Tail length (μm)	% DNA in head	% DNA in tail	Tail moment (μm)
Day 7						
Control	40.20 ± 3.03	35.30 ± 2.20	5.90 ± 0.79	85.67 ± 4.22	14.32 ± 3.10	0.11 ± 0.03
T1	40.52 ± 2.27	34.80 ± 3.0	6.10 ± 0.70	85.33 ± 3.94	14.81 ± 2.17	0.15 ± 0.04
T2	40.97 ± 2.86	34.81 ± 3.12	6.77 ± 0.73	85.08 ± 3.74	14.55 ± 2.27	0.13 ± 0.05
T3	41.81 ± 3.22	33.10 ± 2.80	6.73 ± 1.03	83.16 ± 3.77	16.84 ± 1.70	0.17 ± 0.02
Day 14						
Control	39.97 ± 2.77	34.83 ± 2.89	5.50 ± 0.77	85.07 ± 3.32	13.92 ± 1.30	0.10 ± 0.02
T1	39.17 ± 2.82	35.32 ± 2.51	6.80 ± 1.30	83.84 ± 2.96	16.15 ± 4.10	0.17 ± 0.05
T2	39.10 ± 2.99	33.75 ± 3.25	5.40 ± 1.20	86.18 ± 3.16	13.81 ± 1.80	0.13 ± 0.03
T3	42.70 ± 3.23	31.81 ± 2.33	8.90 ± 1.10	78.13 ± 3.77	21.86 ± 2.10	0.21 ± 0.07
Day 21						
Control	40.30 ± 3.33	34.20 ± 2.70	5.86 ± 1.33	84.86 ± 3.23	14.13 ± 2.10	0.11 ± 0.04
T1	41.27 ± 3.37	29.71 ± 3.07	11.51 ± 1.21	72.08 ± 3.21	27.91 ± 2.90	0.24 ± 0.15
T2	41.21 ± 2.71	30.71 ± 2.91	8.52 ± 1.77	78.31 ± 3.13	21.68 ± 2.80	0.15 ± 0.03
T3	43.22 ± 2.82	27.92 ± 3.19	14.31 ± 1.63	66.11 ± 3.90	33.88 ± 2.70	0.39 ± 0.06
Day 28						
Control	39.89 ± 3.02	34.50 ± 2.90	5.47 ± 1.81	84.95 ± 3.98	14.79 ± 1.76	0.12 ± 0.05
T1	42.19 ± 3.79	27.30 ± 3.37	14.80 ± 1.56	64.22 ± 3.15	35.77 ± 3.23	0.48 ± 0.22
T2	41.37 ± 3.11	30.20 ± 3.18	10.10 ± 1.52	74.93 ± 3.19	25.05 ± 1.84	0.17 ± 0.09
T3	44.71 ± 2.72	23.20 ± 2.81	17.50 ± 2.03	57.09 ± 4.21	42.10 ± 3.17	0.98 ± 0.12

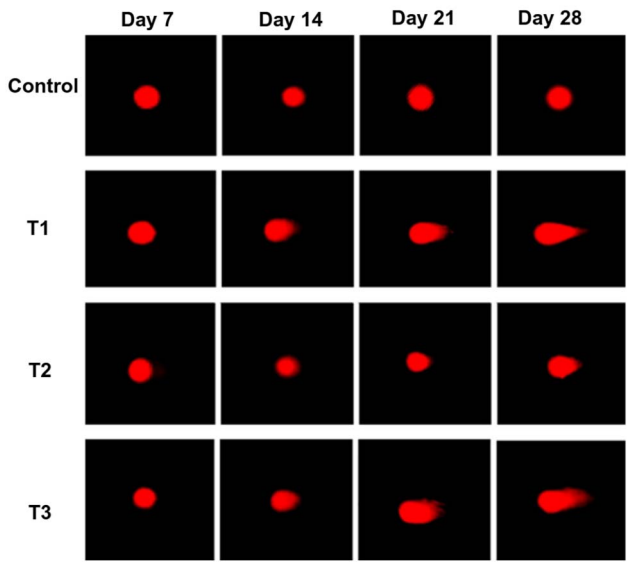

Fig. 6 Representative fluorescence micrographs of DNA damage in zebrafish hepatic cells assessed *via* comet assay following exposure to $NaAsO_2$ and CuO-NPs and their co-exposure captured at 40×.

increases in ROS and MDA were highly associated with antioxidant depletions and genotoxic effects. The strongest correlations were consistently obtained in the T3 group, suggesting potential treatment-dependent or synergistic effects. In contrast, weaker correlations were observed in the control group, implying that the observed interdependencies among biomarkers were specifically enhanced by toxicant exposure. These results underscore the systematic nature of oxidative stress and DNA damage interactions in response to environmental toxicants.

3.9 Synergistic toxicity

The synergism and antagonism of $NaAsO_2$ and CuO-NPs were identified using the Bliss independence model with a 95% confidence interval. We defined synergism, antagonism, and independent relation in terms of the Bliss synergy index (BSI); BSI > 0 indicates synergism, BSI < 0 represents antagonism, and BSI = 0 when two toxicants are independent of each other, as reported in the literature.[49] The Bliss model was applied to oxidative stress biomarkers, antioxidant enzyme activities and genotoxicity endpoints. The total ROS production, MDA and TM established synergism while antioxidant enzymes and AChE exhibited antagonism.

The BSI value for total ROS exceeded 1.2 on the 28th day of co-exposure, indicating a pronounced increase in ROS levels when the two toxicants were combined. In the initial days, the interaction between $NaAsO_2$ and CuO-NPs was additive in nature; however, the synergy became evident with longer exposure periods. The BSI > 1.44 and BSI > 6.0 values for MDA and TM, respectively, indicated synergistic toxicity under co-exposure on the 28th day, as shown in Fig. 9. However, BSI < 0, as evident in the case of SOD, CAT, and AChE activities, indicated antagonistic interactions. This does not mean reduced toxicity. The antagonism in the case of antioxidant enzymes and AChE means that the observed combined enzyme activity is less than the expected enzyme activity under independent actions. It means that co-exposure prevented the expected upregulation of the compensatory defense mechanism. This impaired adaptive response is in alignment with the

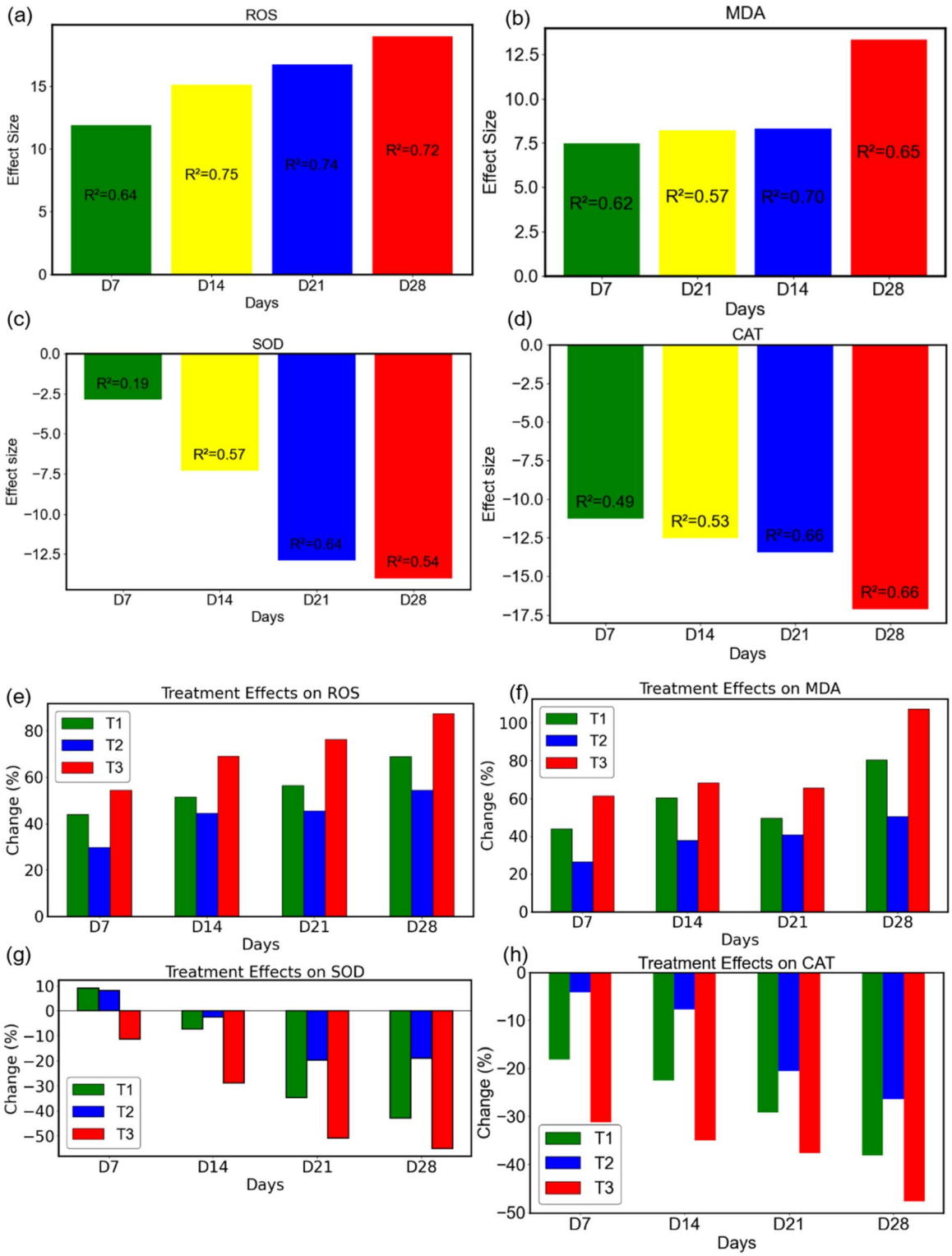

Fig. 7 Linear regression analysis of time and treatment-dependent effects of $NaAsO_2$, CuO-NPs, and their co-exposure on oxidative stress and antioxidant enzymes in zebrafish hepatic tissues. Panels (a–d) show time-dependent effect sizes and regression coefficients (R^2) for (a) ROS, (b) MDA, (c) SOD, (d) CAT across 7, 14, 21, and 28 days of exposure. Panels (e–h) exhibit treatment-specific percentage changes relative to the control for (e) ROS, (f) MDA, (g) SOD, and (h) CAT across different time points under the T1, T2, and T3 treatment groups.

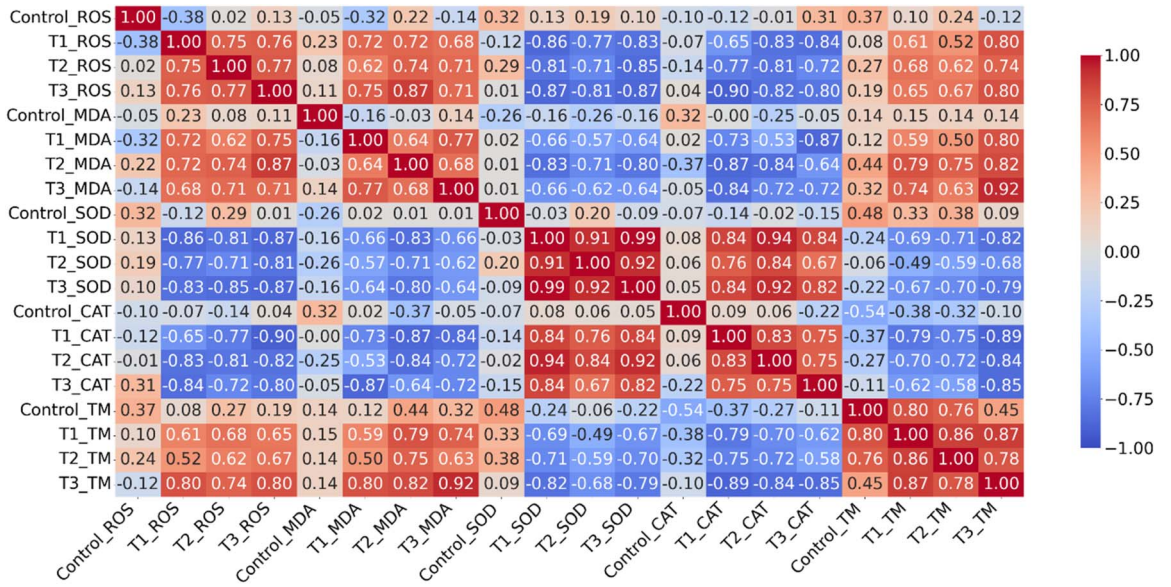

Fig. 8 Correlation heatmap between oxidative stress biomarkers, antioxidant enzyme activities and genotoxicity across various treatment groups in the liver tissue homogenate of adult zebrafish. The red and blue colors indicate positive and negative correlations, respectively, and the color intensity indicates the magnitude of the correlation.

observed experimental stress, neurotoxicity, and progressive damage. Overall, these findings indicated that prolonged co-exposure elicited synergistic oxidative stress and genotoxic effects exceeding additive predictions, accompanied by a weaker antioxidant defense system.

4 Discussion

Environmental toxicants have achieved high importance due to their implications for human health and their omnipresence in aquatic and terrestrial ecosystems. To the best of our knowledge, this study is the first to examine the toxicological effects of sonochemically synthesized CuO-NPs individually and in combination with $NaAsO_2$. This study advances the present knowledge by moving beyond organ-specific toxicity in response to a single toxicant. Previous studies have exclusively focused on the gill, liver and kidney histopathologies, while we identified skeletal muscles to be highly sensitive and progressively susceptible to the combined exposure of toxicants. The application of the Bliss mathematical model to antioxidant defense and neuroprotective enzymes represents a conceptual innovation, integrating mathematical models into toxicological compensation. Additionally, the present study also outlines the impact of environmental toxicants on freshwater fauna individually and in combination with co-occurring contaminants, underscoring their biological importance and supporting several sustainable development goals: SDG-3 (good health and well-being), SDG-6 (clean water and sanitation), and SDG-14 (life below water). Engineered nanomaterials, which in the case of CuO-NPs are produced only by sonochemical methods, have raised concerns over synergistic toxicity through interaction with legacy pollutants in natural aquatic ecosystems. The present study systematically investigates how CuO-NPs interact with $NaAsO_2$ to affect the skeletal muscle architecture, biochemical profiles, and DNA integrity in adult zebrafish, thus providing critical insights into the health and environmental risks associated with mixed exposure. The relative examination of solid particles and dissolved toxicants is comparable with previously reported zebrafish-based toxicological frameworks, where Osborne *et al.* showed that As(III) and nanoscale III–V particles co-exist in aquatic environments and induce oxidative stress-mediated tissue damage. This highlights that solid NPs and metal ion species can produce adverse effects *via* overlapping toxicity pathways.[50] The present study signifies the relevance of simultaneously assessing solid CuO-NPs and dissolved metal ions for realistic freshwater contamination.

The CuO-NPs were synthesized *via* a sonochemical method. The PXRD pattern confirmed monoclinic crystalline forms and is in concordance with the previous literature.[51,52] No impurity peaks were observed in the diffraction data. The Cu–O vibrations were evident in FTIR spectra at peak positions of 512 cm^{-1} and 597 cm^{-1} and are in alignment with the previously reported literature. The broad peak at 3401 cm^{-1} represented –OH stretching due to water molecules.[53] Moreover, the peaks at 1627 cm^{-1} and 1112 cm^{-1} may be due to H–O–H bending[54] and the carbonate or bicarbonate stretching of C–O due to CO_2 encapsulation on the CuO-NPs surface from the environment.[55] There were strong signals of Cu and O in the EDX pattern, which confirmed the elemental composition and purity of NPs. However, the C signal may be attributed to the carbon coating used during sample preparation for SEM. The SRP band at 300 nm is consistent with the previous literature, validating the nanoscale properties of newly synthesized NPs.[56]

There is a size discrepancy between PXRD and SEM analysis; PXRD measures the crystallite size, while SEM quantifies the particle size. Multiple crystalline units arrange themselves in

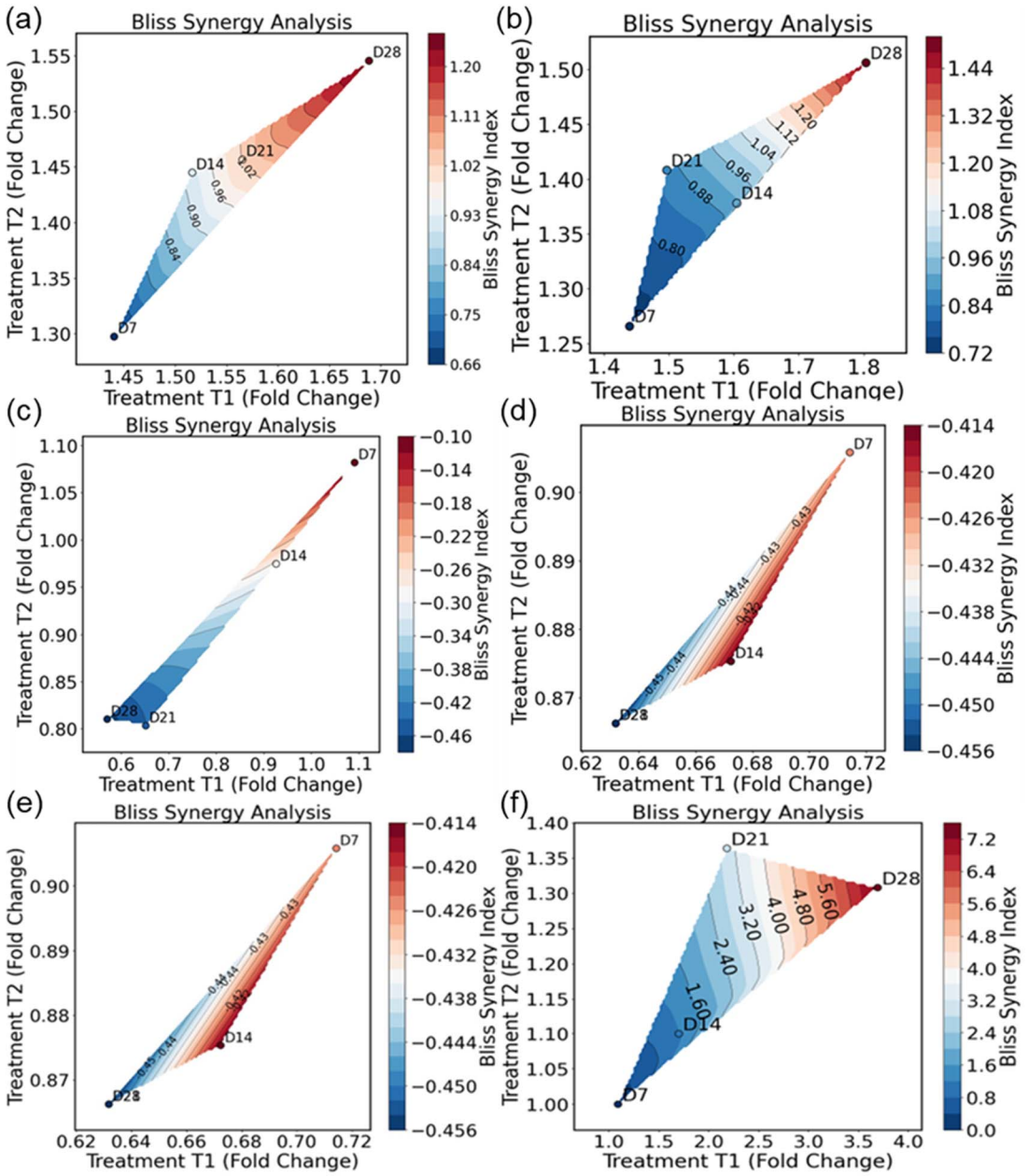

Fig. 9 Quantification of the synergistic toxicity of $NaAsO_2$ and CuO-NPs *via* Bliss synergy analysis in adult zebrafish: effects on (a) ROS production, (b) MDA production, (C) SOD activity, (d) CAT activity, (e) AChE activity, and (f) TM. The Bliss independence model was applied to evaluate interactive effects across exposure durations. Synergistic interactions (BSI > 1.0) were evident for ROS, MDA, and TM, particularly on day 28. However, SOD, CAT, and AChE exhibited antagonistic interactions (BSI < 0), suggesting a preserved antioxidant defense mechanism.

different orientations to form a particle, so the particle size is always larger than the crystallite size and these results are in accordance with the previous literature.[57,58] Additionally, the Debye Scherer equation considers that all the particles are comprised of monocrystalline, spherical crystallites, and does not consider polycrystalline or irregularly shaped crystals, thus contributing to the size variations.[59]

The musculature of zebrafish is of great significance as it plays a role in swimming. It contains a high density of mitochondria as it is an active metabolic site for oxidative phosphorylation. It is highly vulnerable to mitochondrial dysfunction, oxidative stress, and metabolic disruption, as has been discussed in the previous studies.[60,61] The evaluation of damage in skeletal muscles presents sensitive readouts of metabolic and oxidative stress together, which may not be fully understood in classical visceral and respiratory organs. Additionally, the integrity of skeletal muscles is directly correlated with swimming performance, predator avoidance, locomotion, and feeding efficiency.[62] The toxicity examination in skeletal muscles describes organismal fitness levels and survival instincts. Muscle fibers also contain neuromuscular junctions rich in ACHE, supporting the development of a correlation

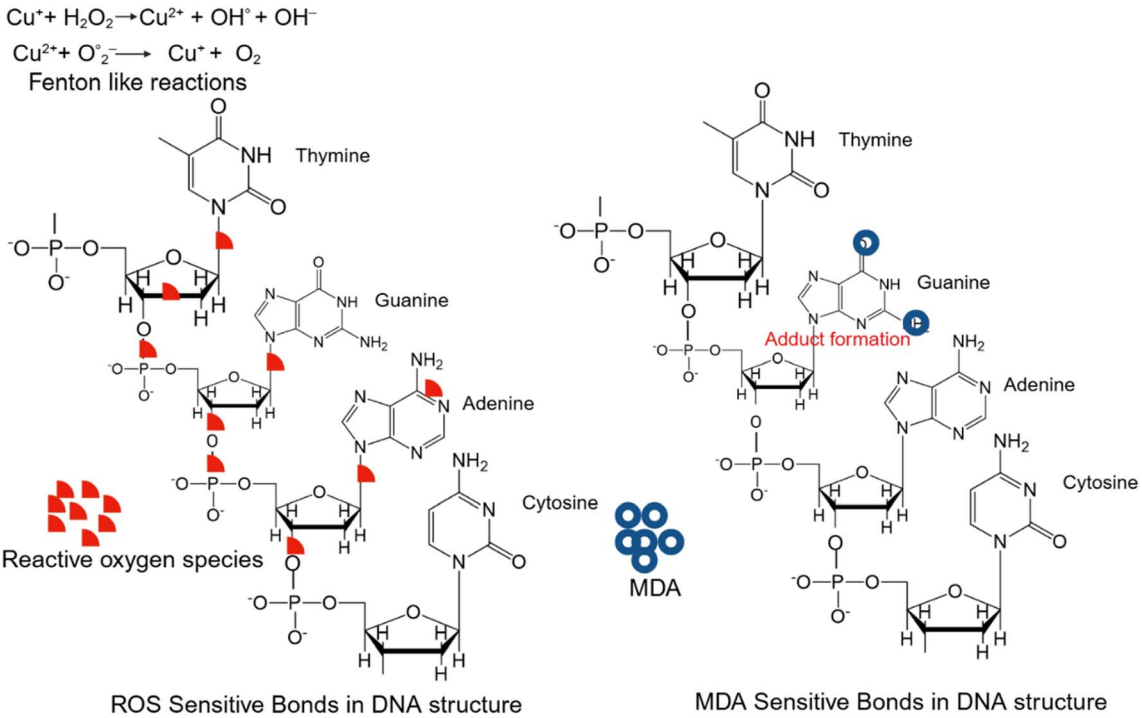

Fig. 10 Probable mechanistic insights into DNA damage due to elevated oxidative stress.

between histopathological changes and neurochemical endpoints, highlighting structural functional relationships. Thus, skeletal muscle histopathology offers a functionally relevant model for assessing systemic toxicity beyond traditional organs.

The muscular histopathology revealed that $NaAsO_2$ and CuO-NPs individually and in combined form induced damage; however, the extent and nature of damage varied in each treatment. These damages may be attributed to multiple factors such as mitochondrial dysfunction, oxidative stress, and gene expression dysregulation. The impaired mitochondria may be a central focus of histopathological damage in all treatments since necrosis is evident in all of them. The disruption of the respiratory chain due to toxicants may lead to reduced adenosine tri-phosphate (ATP) generation, thereby disturbing cellular homeostasis and energy failure leading to necrosis of myofibers.[63] Recently, Zhang *et al.* reported that chemically synthesized CuO-NPs disrupt mitochondrial membrane potential and energy production in zebrafish, thus disrupting the overall fiber structural and functional integrity.[64] The CuO-NPs may influence the gene expression of apoptotic signaling pathways and inflammatory cytokines, as has been reported in the literature.[65] In contrast, Ro *et al.* reported that As might disrupt mitochondrial function, glucose metabolism, and the NF-kB signaling pathway in muscular tissues.[66]

$NaAsO_2$ also disrupts the expression of myogenic regulatory factors, thereby interfering with muscle regeneration and compromising physiological functions.[67] The combined exposure in the T3 group exhibited the highest degree of damage, reflecting the anomalies of both T1 and T2 groups. The severity of this damage may be attributed to the presence of two toxicants at the same time and exposure duration, thus resulting in compromised muscular health.

Another mechanism that can directly contribute to the muscular damage is high oxidative stress and a compromised antioxidant defense system. The rise in oxidative stress biomarkers leads to the generation of free radicals and these free radicals directly or indirectly damage muscular tissues. The CuO-NPS may exacerbate oxidative damage in animal bodies, as copper has the potential to undergo the Haber–Weiss and Fenton reactions. The CuO-NPs have the potential to disrupt biological membranes *via* lipid peroxidation and protein aggregation.[40] Similarly, $NaAsO_2$ elevates ROS and MDA levels, consistent with the previous studies,[68,69] contributing to oxidative damage and subsequent myofiber degeneration.

The combined exposure to $NaAsO_2$ and CuO-NPs elicited profound oxidative and enzymatic disturbances in zebrafish hepatic tissues, pointing to a synergistic toxicological interaction. $NaAsO_2$ is a notorious oxidative stress inducer, while sonochemically synthesized CuO-NPs have also responded in the same way. Both chemicals elevated the ROS and MDA levels. These oxidative insults were accompanied by a marked suppression of antioxidant enzymes, including SOD and CAT. Reductions in AChE activity further highlighted the neurotoxic effects, indicating compromised neuromuscular functions. These findings align with previous reports that arsenic and metal oxide NPs individually disrupt redox balance and antioxidant defenses.[70–74] However, their co-exposure in this study has highlighted amplified oxidative damage, suggesting synergetic toxicity. This disruption of enzymatic and neurotransmitter

regulation under oxidative stress highlights the broader physiological consequences of ECs, underscoring the need for regulatory scrutiny and further mechanistic investigation.

DNA damage was quantified using the comet assay, a widely recognized, rapid, affordable, versatile and sensitive method for measuring DNA damage in eukaryotic cells. $NaAsO_2$ and sonochemically synthesized CuO-NPs increased ROS and MDA levels, and have the potential to directly attack various loci on DNA strands and the ability to damage their integrity. The disruption of oxidant–antioxidant homeostasis compromises the intrinsic cellular defense mechanisms, resulting in DNA damage. The depletion of antioxidants is an oxidative insult to DNA and in response, the cell activates a network of DNA damage response pathways targeted at repair. However, chronic and sustained oxidative exposure, as observed under co-exposure conditions, leads to the accumulation of DNA damage that predisposes cells to apoptosis, mutagenesis, or senescence.[75–81] The underlying mechanism for DNA damage is shown in Fig. 10.

The small size of CuO-NPs may be another major contributing factor to the overall toxicity. Previous studies have reported that nanomaterial-induced toxicity is strongly size dependent. Karlsson *et al.* reported that CuO-NPs with an average size of 42 nm demonstrated greater toxicity than microparticles, exhibiting reduced cell viability, pronounced DNA damage, and mitochondrial dysfunction.[82] Another study showed that CuO-NPs caused DNA damage *via* lipid peroxidation and oxidative stress, leading to the activation of apoptosis in pulmonary epithelial cells.[83] Miao *et al.* further described in detail that smaller-sized nanoparticles had large surface areas that enhanced their overall interaction with the biological system. Nanomaterials below 20 nm in size can easily cross biological membranes, contributing to intense *in vivo* toxicity. They disrupt the integrity of tight junctions present between cells and modulate inflammatory responses.[84] In support of this size-dependent toxicity, Jimeno-Romero *et al.* added that smaller sized silver nanoparticles (20 nm) were more toxic for muscle fibers in comparison to 100 nm particles in *Mytilus galloprovincialis*.[85] Collectively, these studies indicate that reduced CuO-NP size promotes cellular penetration and biological reactivity, thereby amplifying size-mediated toxicity.

Moreover, in zebrafish, the toxicity of $NaAsO_2$ is concentration-dependent. The chronic exposure of $NaAsO_2$ (50–500 μg L^{-1} for 30 days) induced alterations to brain nuclei, synapses, and organelles, with higher damage reported in higher As concentrations.[86] Piyushbhai *et al.* reported that the extent of damage for embryogenesis, teratogenicity, developmental retardation, enzyme activities, inflammatory cytokines, and behavioral anomalies was progressively altered in zebrafish embryos with increasing $NaAsO_2$ concentrations.[87] Li *et al.* described that the viability of zebrafish embryos was reduced significantly at higher concentrations of $NaAsO_2$.[88] Thus, these findings elucidate that $NaAsO_2$ toxicity in zebrafish is concentration-dependent, and future research should aim to explore its concentration-dependent interactive effects with CuO-NPs, with exclusive focus on bioavailability, molecular pathways, and NP behavior.

The findings of the present study are in alignment with previous studies where it has been reported that CuO-NPs caused histopathological anomalies in the intestines, gills, liver, and muscle, and neurotoxicity in *Cyprinus carpio* and *Danio rerio*.[40,89] Moreover, the oxidative stress response due to CuO-NPs is similar to that in the study by Ganesan *et al.*, on zebrafish embryos.[90] However, Sun *et al.* demonstrated that $NaAsO_2$ induced oxidative stress and histopathological anomalies in gills.[42] Ma *et al.* also reported that $NaAsO_2$ had the potential to induce histopathological changes in the brain, but our study exposed it in muscular tissues.[86] All the earlier studies exclusively focused on individual toxicant effects; however, this study has adopted a more comprehensive approach by evaluating ECs in a new approach of evaluating solid nanoparticles and dissolved toxicants. Overall, these findings present strong evidence that treatment with the sonochemically fabricated CuO-NPs, both individually and in co-exposure with $NaAsO_2$, exerts significant toxic effects on zebrafish. All the results, exclusively histopathological anomalies, oxidative stress, disturbance in antioxidant enzymes activities and genotoxicity, underscore the potential for environmental concern regarding CuO-NPs. These NPs, when interacting with $NaAsO_2$ in natural waterbodies, can synergistically exacerbate the severity of the toxicological damage. These findings highlight a new toxicant that may place aquatic fauna at risk, and emphasize the need for regulatory mechanisms for their safer application. In summary, this study provides critical insights into the environmental risks posed by CuO-NPs in combination with $NaAsO_2$. It underscores their significance for advancing the SDGs and regulatory policies to protect freshwater biodiversity.

4.1 Limitations of the study

This study was designed to investigate the toxic effects of CuO-NPs alone and in combination with $NaAsO_2$ on zebrafish adults. Limitations include the use of only one non-lethal concentration of $NaAsO_2$ and CuO-NPs, limiting the ability to conduct dose and threshold analyses. In this study, we did not monitor the changing conditions of the CuO-NPs during the treatment period (*e.g.*, aggregation or partial solutions of the particles) or how they changed over time (*i.e.*, dynamic transformation of NPs size, *etc.*). Furthermore, as we utilized an adult zebrafish model with specified controlled conditions, such an experimental design may not adequately reflect the relative sensitivity among lifecycle stages or complex interactions present in natural aquatic/terrestrial environments. As a consequence of our use of DMSO as a solvent carrier (to disperse NPs) at a very low concentration (0.001%) that has been reported to be non-toxic, some of the solvent-mediated effects could not necessarily be ruled out. Despite these limitations, the original design of the experiments was focused specifically on establishing separate comparisons of the toxicities produced by $NaAsO_2$ and CuO-NPs *versus* their combined toxicity. Future experiments employing multiple dosing regimens, comparisons across developmental stages, and analyses of the dynamic transformation of nanoparticles into the exposure solutions will provide greater mechanistic insights.

5 Conclusion

This study has focused on systematically examining the effects of individual exposure and co-exposure to $NaAsO_2$ and sonochemically synthesized CuO-NPs on adult zebrafish as a model organism. The average crystallite size of the newly synthesized NPs was 10.56 nm, with a monoclinic crystalline structure. The average particle size of the NPs was 41.66 nm, with a clear, sharp surface plasmon resonance band at 250 nm.

The CuO-NPs induced significant histopathological alterations in muscular tissues individually and in combination with $NaAsO_2$ in an exposure duration-dependent manner. The key histomorphological changes observed were necrosis, edema, swelling, and delocalized nuclei, with the greatest skeletal muscle damage occurring on the 28th day of exposure. The co-exposed group on the 28th day of exposure demonstrated the most pronounced oxidative stress, impairment of the antioxidant defense mechanism, and DNA damage. The CuO-NPs also induced oxidative stress and significantly suppressed the antioxidant defense system in hepatic tissues, resulting in extensive DNA strand breakage (TM $= 0.98 \pm 0.12$ on the 28th day in the T3 group). There were strong, significant correlations ($P = 0.05$) between oxidative stress biomarkers, antioxidant enzyme activities, and tail moments. The Bliss synergy model revealed the pattern of synergism and antagonism between different variables. Collectively, these findings provide mechanistic insights into how combined toxicant exposures disrupt biological defenses and promote tissue damage at different exposure durations.

Ethics approval

This study makes use of animals, and the experimental protocol was approved (#BEC-FBS-QAU2024-657) by the ethical board of Quaid-i-Azam University, Islamabad, Pakistan.

Author contributions

Aq. H. and A. H. are first authors. Conceptualization: A. H., M. I. Z., M. B. T., I. A. K; data curation: A. H., A. A. N. K.; formal analysis: Z. S., M. M., N. K., I. A. K; investigation: Aq. H, A. H, A. A; methodology: Aq. H., A. H., M. I. Z., M. B. T.; software: A. H., N. K. Resources: M. I. Z; writing—original draft: Aq. H., A. H, M. I. Z., M. B. T.; writing—review and editing: M. I. Z., M. B. T., I. A. K.; funding acquisition; M. I. Z. All authors have read and agreed to the published version of the manuscript.

Conflicts of interest

The authors declare that they have no known competing financial interests or personal relationships that could have appeared to influence the work reported in this paper.

Data availability

All data generated or analyzed during this study are encompassed in this article and are available from the corresponding author.

Supplementary information (SI) is available. See DOI: https://doi.org/10.1039/d5ra09469k.

Acknowledgements

This study was financially supported by contributions from the University Research Funds (URF-FBS-QAU/2024-92) of Quaid-i-Azam University, Islamabad. We wish to express our indebtedness to the technical staff of the Chemistry department for the work on XRD and FTIR analyses. We acknowledge exclusive support from the National Center of Physics for the SEM-EDS analysis of samples.

References

1 I. B. Gomes, *J. Appl. Microbiol.*, 2025, **136**, lxaf064.
2 C. K. Singh, K. K. Sodhi, N. V, V. Rajagopalan, S. Sharma, J. Kaur and Y. Kumar, *Discov. Catal.*, 2025, **2**, 9.
3 P. K. Singh, U. Kumar, I. Kumar, A. Dwivedi, P. Singh, S. Mishra, C. S. Seth and R. K. Sharma, *Environ. Sci. Pollut. Res.*, 2024, **31**, 56428–56462.
4 M. Hait, N. K. Kashyap and A. K. Bhardwaj, in *Biomonitoring of Pollutants in the Global South*, Springer, 2024, pp. 39–87.
5 V. Saxena, *Water, Air, Soil Pollut.*, 2025, **236**, 73.
6 S. C. Izah, S. T. Abdelkhalek, M. C. Ogwu and H. Hamidifar, in *Biomonitoring of Pollutants in the Global South*, Springer, 2024, pp. 3–36.
7 N. Talreja, C. Hegde, E. M. Kumar and M. Chavali, *Green Technologies for Industrial Contaminants*, 2025, pp. 119–149.
8 N. Morin-Crini, E. Lichtfouse, G. Liu, V. Balaram, A. R. L. Ribeiro, Z. Lu, F. Stock, E. Carmona, M. R. Teixeira and L. A. Picos-Corrales, in *Emerging Contaminants, Vol. 1: Occurrence and Impact*, Springer, 2021, pp. 1–111.
9 M. Patel, R. Kumar, K. Kishor, T. Mlsna, C. U. Pittman Jr and D. Mohan, *Chem. Rev.*, 2019, **119**, 3510–3673.
10 T. Ruan, P. Li, H. Wang, T. Li and G. Jiang, *Chem. Rev.*, 2023, **123**, 10584–10640.
11 D. Cserbik, P. E. Redondo-Hasselerharm, M. J. Farré, J. Sanchís, A. Bartolomé, A. Paraian, E. M. Herrera, J. Caixach, C. M. Villanueva and C. Flores, *npj Clean Water*, 2023, **6**, 16.
12 D. Savoca and A. Pace, *Int. J. Mol. Sci.*, 2021, **22**, 6276.
13 F. Wang, L. Xiang, K. S.-Y. Leung, M. Elsner, Y. Zhang, Y. Guo, B. Pan, H. Sun, T. An and G. Ying, *Innovation*, 2024, **5**, 1–3.
14 R. Y. Hiranmai and M. Kamaraj, *Phys. Sci. Rev.*, 2023, **8**, 2219–2242.
15 V. Singh, H. Sable, M. Ghalley and K. Tenzin, in *Occurrence, Distribution and Toxic Effects of Emerging Contaminantsx*, CRC Press, 2024, pp. 134–167.
16 A. O. Asuku, M. T. Ayinla, A. J. Ajibare, M. B. Adeyemo and R. O. Adeyemo, in *Emerging Contaminants in Food and Food Products*, CRC Press, 2024, pp. 236–250.
17 M. E. Street, A.-M. Shulhai, R. Rotondo, G. Giannì and C. Caffarelli, *Front. Nutr.*, 2023, **10**, 1120293.
18 T.-Y. Suman, S.-Y. Kim, D.-H. Yeom and J. Jeon, *Toxics*, 2022, **10**, 54.

19 W. Jadaa and H. Mohammed, *J. Ecol. Eng.*, 2023, **24**, 249–271.
20 Y. Xie, L. Yu, L. Chen, C. Chen, L. Wang, F. Liu, Y. Liao, P. Zhang, T. Chen and Y. Yuan, *Sci. China: Chem.*, 2024, **67**, 3515–3577.
21 P. Talukder, R. Ray, M. Sarkar, A. Das and S. Chakraborty, *Environ. Qual. Manage.*, 2024, **33**, 595–610.
22 N. B. Saidon, R. Szabó, P. Budai and J. Lehel, *Environ. Pollut.*, 2024, **340**, 122815.
23 B. Zhou, T. Zhang and F. Wang, *Appl. Sci.*, 2023, **13**, 8439.
24 S. Ray and S. T. Shaju, *Environ. Anal. Health Toxicol.*, 2023, **38**, e2023017.
25 M. Yousaf, *The Combined Effects or Arsenic Cadmium and Mercury on Hepatocarcinoma and Neuroblastoma Cells In Vitro*, University of Pretoria, South Africa, 2018.
26 R. Yan, J. Ding, Y. Wei, Q. Yang, X. Zhang, H. Huang, Z. Shi, Y. Feng, H. Li and H. Zhang, *Antioxidants*, 2022, **11**, 1301.
27 N. Abu Bakar, W. N. Wan Ibrahim, C. A. Che Abdullah, N. F. Ramlan, K. Shaari, S. Shohaimi, A. Mediani, N. S. Nasruddin, C.-H. Kim and S. M. Mohd Faudzi, *Toxics*, 2022, **10**, 493.
28 J. Kanungo, N. C. Twaddle, C. Silva, B. Robinson, M. Wolle, S. Conklin, S. MacMahon, Q. Gu, I. Edhlund and L. Benjamin, *Neurosci. Lett.*, 2023, **795**, 137042.
29 R. Yan, J. Ding, Q. Yang, X. Zhang, J. Han, T. Jin, S. Shi, X. Wang, Y. Zheng and H. Li, *Ecotoxicol. Environ. Saf.*, 2023, **253**, 114666.
30 N. Akhtar, S. Malik, F. Muhammad and Z. Ullah, *Nano Select*, 2025, e70015.
31 M. H. Saleem, U. Ejaz, M. Vithanage, N. Bolan and K. H. Siddique, *Clean Technol. Environ. Policy*, 2024, 1–26.
32 B. Negrini, P. Floris, C. D'Abramo, S. A. Aldaghi, M. Costamagna, M. Perucca, M. Saibene, I. Perelshtein, A. Colombo and P. Bonfanti, *Discover Nano*, 2025, **20**, 51.
33 A. Hamza, M. B. Taj, M. M. Alsabban, A. M. Altowerqi, S. Jahan, A. Afzal and S. Alghamdi, *RSC Adv.*, 2025, **15**, 34016–34038.
34 R. M. David, H. S. Jones, G. H. Panter, M. J. Winter, T. H. Hutchinson and J. K. Chipman, *Chemosphere*, 2012, **88**, 912–917.
35 J. Hoyberghs, C. Bars, M. Ayuso, C. Van Ginneken, K. Foubert and S. Van Cruchten, *Front. Toxicol.*, 2021, **3**, 804033.
36 N. Yakubu, S. Ahmad, H. Usman, H. Abubakar and A. Amuzat, *IOSR J. Pharm. Biol. Sci.*, 2018, **8**, 18–27.
37 K. D. Brahman, T. G. Kazi, J. A. Baig, H. I. Afridi, A. Khan, S. S. Arain and M. B. Arain, *Chemosphere*, 2014, **100**, 182–189.
38 J. Sultana, A. Farooqi and U. Ali, *Environ. Monit. Assess.*, 2014, **186**, 1241–1251.
39 J. Hallauer, X. Geng, H.-C. Yang, J. Shen, K.-J. Tsai and Z. Liu, *Zebrafish*, 2016, **13**, 405–412.
40 R. Mani, S. Balasubramanian, A. Raghunath and E. Perumal, *Environ. Sci. Pollut. Res.*, 2020, **27**, 27358–27369.
41 C. Zhang, Y. Li, H. Yu, L. Ye, T. Li, X. Zhang, C. Wang, P. Li, H. Ji and Q. Gao, *Sci. Total Environ.*, 2023, **863**, 161005.
42 H.-J. Sun, W.-J. Zhao, X.-Q. Teng, S.-P. Shu, S.-W. Li, H.-C. Hong and D.-X. Guan, *Ecotoxicol. Environ. Saf.*, 2020, **200**, 110743.
43 F. He, *Bio-protocol*, 2011, e45.
44 I. Hayashi, Y. Morishita, K. Imai, M. Nakamura, K. Nakachi and T. Hayashi, *Bio-Protoc.*, 2007, **631**, 55–61.
45 J. Wright, H. Colby and P. Miles, *Arch. Biochem. Biophys.*, 1981, **206**, 296–304.
46 M. Iqbal, S. Sharma, H. Rezazadeh, N. Hasan, M. Abdulla and M. Athar, *Redox Rep.*, 1996, **2**, 385–391.
47 B. Shao, L. Zhu, M. Dong, J. Wang, J. Wang, H. Xie, Q. Zhang, Z. Du and S. Zhu, *Ecotoxicology*, 2012, **21**, 1533–1540.
48 D. Debnath and T. K. Mandal, *J. Appl. Toxicol.*, 2000, **20**, 197–204.
49 Q. Liu, X. Yin, L. R. Languino and D. C. Altieri, *Stat. Biopharm. Res.*, 2018, **10**, 112–122.
50 O. J. Osborne, S. Lin, W. Jiang, J. Chow, C. H. Chang, Z. Ji, X. Yu, S. Lin, T. Xia and A. E. Nel, *Environ. Sci.: Nano*, 2017, **4**, 1350–1364.
51 S. Sagadevan, K. Pal and Z. Z. Chowdhury, *J. Mater. Sci.: Mater. Electron.*, 2017, **28**, 12591–12597.
52 T. Banu, M. Jamal and F. Gulshan, *Results Mater.*, 2023, **19**, 100419.
53 A. El-Trass, H. ElShamy, I. El-Mehasseb and M. El-Kemary, *Appl. Surf. Sci.*, 2012, **258**, 2997–3001.
54 Z. N. Kayani, M. Umer, S. Riaz and S. Naseem, *J. Electron. Mater.*, 2015, **44**, 3704–3709.
55 N. B. Tanvir, O. Yurchenko, C. Wilbertz and G. Urban, *J. Mater. Chem. A*, 2016, **4**, 5294–5302.
56 A. Qona'ah, M. M. Suliyanti, E. Hidayanto and A. Khumaeni, *Results Chem.*, 2023, **6**, 101042.
57 J. Becker, K. R. Raghupathi, J. S. Pierre, D. Zhao and R. T. Koodali, *J. Phys. Chem. C*, 2011, **115**, 13844–13850.
58 V. Uvarov and I. Popov, *Mater. Charact.*, 2007, **58**, 883–891.
59 C. Dazon, O. Witschger, S. Bau, V. Fierro and P. L. Llewellyn, *Environ. Sci.: Nano*, 2019, **6**, 152–162.
60 D. I. Bassett and P. D. Currie, *Hum. Mol. Genet.*, 2003, **12**, R265–R270.
61 I. Ferrandino, T. Capriello, L. M. Félix, G. Di Meglio, D. Santos and S. M. Monteiro, *Environ. Toxicol. Pharmacol.*, 2022, **94**, 103934.
62 H. F. Olivares-Rubio and E. Arce, *Environ. Biol. Fishes*, 2023, **106**, 1149–1176.
63 S. Naz, A. Gul and M. Zia, *IET Nanobiotechnol.*, 2020, **14**, 1–13.
64 M. Zhang, W. Wang, D. Zhang, Y. Zhang, Z. Yang, Y. Li, F. Fang, Y. Xue and Y. Zhang, *Food Chem. Toxicol.*, 2024, **185**, 114441.
65 H. M. Abdel-Latif, M. A. Dawood, S. F. Mahmoud, M. Shukry, A. E. Noreldin, H. A. Ghetas and M. A. Khallaf, *Animals*, 2021, **11**, 652.
66 S.-H. Ro, J. Bae, Y. Jang, J. F. Myers, S. Chung, J. Yu, S. K. Natarajan, R. Franco and H.-S. Song, *Antioxidants*, 2022, **11**, 689.
67 C. Zhang, R. Ferrari, K. Beezhold, K. Stearns-Reider, A. D'Amore, M. Haschak, D. Stolz, P. D. Robbins, A. Barchowsky and F. Ambrosio, *Stem Cells*, 2016, **34**, 732–742.
68 H. M. Abdou, A. M. Saad, H.-T. A. E. Abd Elkader and A. E. Essawy, *Toxicol. Res.*, 2024, **13**, tfae203.

69 S. Gencer, C. Gür, M. İleritürk, S. Küçükler, N. Akaras, H. Şimşek and F. M. Kandemir, *J. Biochem. Mol. Toxicol.*, 2024, **38**, e23863.
70 T. Tasci, B. Orta-Yilmaz, Y. Aydin and M. Caliskan, *Toxicol. Res.*, 2024, **13**, tfae128.
71 S. Akbari, F. T. Amiri, M. Naderi, F. Shaki and M. Seyedabadi, *Toxicology*, 2022, **470**, 153148.
72 N. N. Farshori, M. A. Siddiqui, M. M. Al-Oqail, E. S. Al-Sheddi, S. M. Al-Massarani, M. Ahamed, J. Ahmad and A. A. Al-Khedhairy, *Biol. Trace Elem. Res.*, 2022, **200**, 5042–5051.
73 W. Shaoyong, W. Wang, B. Pan, R. Liu, L. Yin, R. Wangjie, H. Tian, Y. Wang and M. Jin, *ACS Nano*, 2024, **18**, 20541–20555.
74 H. P. Borase, R. S. Singhal and S. V. Patil, *Environ. Sci. Pollut. Res.*, 2024, **31**, 54325–54337.
75 R. Mohamed, I. Hasan, Z. M. Maher and H. Ahmed, *SVU-Int. J. Vet. Sci.*, 2023, **6**, 93–113.
76 W. A. Ghonimi, M. A. Alferah, N. Dahran and E. S. El-Shetry, *Environ. Sci. Pollut. Res.*, 2022, **29**, 81923–81937.
77 B. Jarrar, M. Almansour, Q. Jarrar, A. Al-Doaiss, S. Y. Lee and D. Boudemagh, *Nanotechnol. Rev.*, 2024, **13**, 20240122.
78 A. Boyadzhiev, S. A. Solorio-Rodriguez, D. Wu, M.-L. Avramescu, P. Rasmussen and S. Halappanavar, *Nanomaterials*, 2022, **12**, 1844.
79 Q. Qian, Y. Chen, J.-Q. Wang, D.-Q. Yang, C. Jiang, J. Sun, J. Dong and G.-C. Li, *Mutat. Res., Genet. Toxicol. Environ. Mutagen.*, 2021, **867**, 503368.
80 F. D. Gökalp, O. Doğanlar, Z. B. Doğanlar and U. Güner, *Drug Chem. Toxicol.*, 2022, **45**, 1158–1167.
81 A. A. González Núñez, J. P. Ferro, L. B. Campos, B. L. Eissa, M. M. Mastrángelo, L. Ferrari and N. A. Ossana, *Environ. Toxicol. Chem.*, 2022, **41**, 1246–1259.
82 H. L. Karlsson, J. Gustafsson, P. Cronholm and L. Möller, *Toxicol. Lett.*, 2009, **188**, 112–118.
83 A. Ahmad, N. Rasheed, N. Banu and G. Palit, *Stress*, 2010, **13**, 356–365.
84 C. Miao, P. Jia, C. Luo, J. Pang, L. Xiao, T. Zhang, J. Duan, Y. Li and Z. Sun, *Ecotoxicol. Environ. Saf.*, 2024, **271**, 115910.
85 A. Jimeno-Romero, E. Bilbao, U. Izagirre, M. Cajaraville, I. Marigómez and M. Soto, *Nanotoxicology*, 2017, **11**, 168–183.
86 H. Ma, W. Yang, Y. Li, J. Li, X. Yang, Y. Chen, Y. Ma, D. Sun and H. Sun, *Ecotoxicol. Environ. Saf.*, 2024, **273**, 116107.
87 M. K. Piyushbhai, A. Binesh, S. Shanmugam and K. Venkatachalam, *Biol. Trace Elem. Res.*, 2023, **201**, 3487–3496.
88 D. Li, C. Lu, J. Wang, W. Hu, Z. Cao, D. Sun, H. Xia and X. Ma, *Aquat. Toxicol.*, 2009, **91**, 229–237.
89 J. Zhao, Z. Wang, X. Liu, X. Xie, K. Zhang and B. Xing, *J. Hazard. Mater.*, 2011, **197**, 304–310.
90 S. Ganesan, N. Anaimalai Thirumurthi, A. Raghunath, S. Vijayakumar and E. Perumal, *J. Appl. Toxicol.*, 2016, **36**, 554–567.